Article

Neuron

Synaptic Vesicle Recycling Pathway Determines Neurotransmitter Content and Release Properties

Highlights

- Dopamine neurons release glutamate and dopamine with different probability
- Coreleased glutamate and dopamine differ in coupling to presynaptic Ca^{2+} channels
- Neurons make two types of synaptic vesicle that differ in response to stimulation
- AP-3 is required specifically for formation of synaptic vesicles storing dopamine

Authors

Kätlin Silm, Jing Yang, Pamela F. Marcott, ..., Amy H. Newman, Christopher P. Ford, Robert H. Edwards

Correspondence

robert.edwards@ucsf.edu

In Brief

In this work on glutamate corelease by dopamine neurons, Silm et al. show that an individual neuron expresses two classes of synaptic vesicle that form through distinct mechanisms and transmit distinct information due to differences in frequency dependence.

Silm et al., 2019, Neuron *102*, 786–800
May 22, 2019
https://doi.org/10.1016/j.neuron.2019.03.031

CellPress

CellPress

Neuron
Article

Synaptic Vesicle Recycling Pathway Determines Neurotransmitter Content and Release Properties

Kätlin Silm,[1,6] Jing Yang,[1,6] Pamela F. Marcott,[2] Cedric S. Asensio,[1,5] Jacob Eriksen,[1] Daryl A. Guthrie,[3] Amy H. Newman,[3] Christopher P. Ford,[2,4] and Robert H. Edwards[1,7,*]

[1]Departments of Neurology and Physiology, Graduate Programs in Neuroscience and Cell Biology, Kavli Institute for Fundamental Neuroscience, Weill Institute for the Neurosciences, UCSF School of Medicine, San Francisco, CA 94143, USA
[2]Department of Physiology and Biophysics, Case Western Reserve University School of Medicine, Cleveland, OH 44106, USA
[3]Medicinal Chemistry Section, Molecular Targets and Medications Discovery Branch, National Institutes of Drug Abuse - Intramural Research Program, Baltimore, MD 21224, USA
[4]Department of Pharmacology, University of Colorado School of Medicine, Anschutz Medical Campus, Aurora, CO 80045, USA
[5]Present address: Department of Biological Sciences, University of Denver, Denver, CO 80210, USA
[6]These authors contributed equally
[7]Lead Contact
*Correspondence: robert.edwards@ucsf.edu
https://doi.org/10.1016/j.neuron.2019.03.031

SUMMARY

In contrast to temporal coding by synaptically acting neurotransmitters such as glutamate, neuromodulators such as monoamines signal changes in firing rate. The two modes of signaling have been thought to reflect differences in release by different cells. We now find that midbrain dopamine neurons release glutamate and dopamine with different properties that reflect storage in different synaptic vesicles. The vesicles differ in release probability, coupling to presynaptic Ca^{2+} channels and frequency dependence. Although previous work has attributed variation in these properties to differences in location or cytoskeletal association of synaptic vesicles, the release of different transmitters shows that intrinsic differences in vesicle identity drive different modes of release. Indeed, dopamine but not glutamate vesicles depend on the adaptor protein AP-3, revealing an unrecognized linkage between the pathway of synaptic vesicle recycling and the properties of exocytosis. Storage of the two transmitters in different vesicles enables the transmission of distinct signals.

INTRODUCTION

Signaling by neuromodulators such as monoamines differs in multiple ways from signaling by the classic neurotransmitters glutamate and GABA. Release of glutamate and GABA at synaptic contacts activates fast ionotropic receptors that provide precise information about timing. In contrast, monoamines activate slower G-protein-coupled receptors, and dopamine neurons form *en passant* presynaptic boutons, often without clear postsynaptic element (Hattori et al., 1991). As a result, these cells have been thought to signal through changes in the extracellular concentration of dopamine, which generally reflects firing rate rather than timing. The difference between synaptic and volume transmission has thus been considered to reflect the properties of the receptors (ionotropic versus metabotropic) and their distance from the release site. However, differences in the mode of transmission also impose distinct requirements on the properties of release. Temporal coding requires fast, synchronous release. In contrast, frequency coding requires sustained release at rates proportionate to firing.

Midbrain dopamine neurons fire in two patterns, tonic (4–5 Hz) and bursting (~20 Hz), and the dopamine release that signals unexpected reward and promotes movement depends on burst firing (Howe and Dombeck, 2016; Schultz et al., 1997). Indeed, dopamine release increases greatly with stimulation frequency (Koranda et al., 2014; Sulzer et al., 2016), suggesting a low release probability that minimizes vesicle depletion and enables release to follow firing rate (Dittman et al., 2000). In midbrain dopamine neurons, the Ca^{2+}-binding protein calbindin indeed reduces the coupling of synaptic vesicles to presynaptic Ca^{2+} channels (Pan and Ryan, 2012), which reduces release probability. In principle, this mechanism would be expected to impair the regulated exocytic release of any classic transmitter by these same cells.

However, many neurons including dopamine neurons corelease at least two different classic transmitters (El Mestikawy et al., 2011; Hnasko and Edwards, 2012; Tritsch et al., 2016). In some cases, release of both occurs from the same synaptic vesicles (Chaudhry et al., 1998; Jonas et al., 1998; Ren et al., 2011; Tritsch et al., 2012) and hence with the same properties. One transmitter can promote packaging of the other: vesicular glutamate transporter VGLUT2 promotes the storage of dopamine by mesolimbic dopamine projections (Birgner et al., 2010; Hnasko et al., 2010) and VGLUT3 the storage of acetylcholine (ACh) by cholinergic interneurons in the striatum (Gras et al., 2008; Nelson et al., 2014). This phenomenon requires expression of the two transporters on the same synaptic vesicles. In this case, the two transmitters activate different receptors (Lamotte

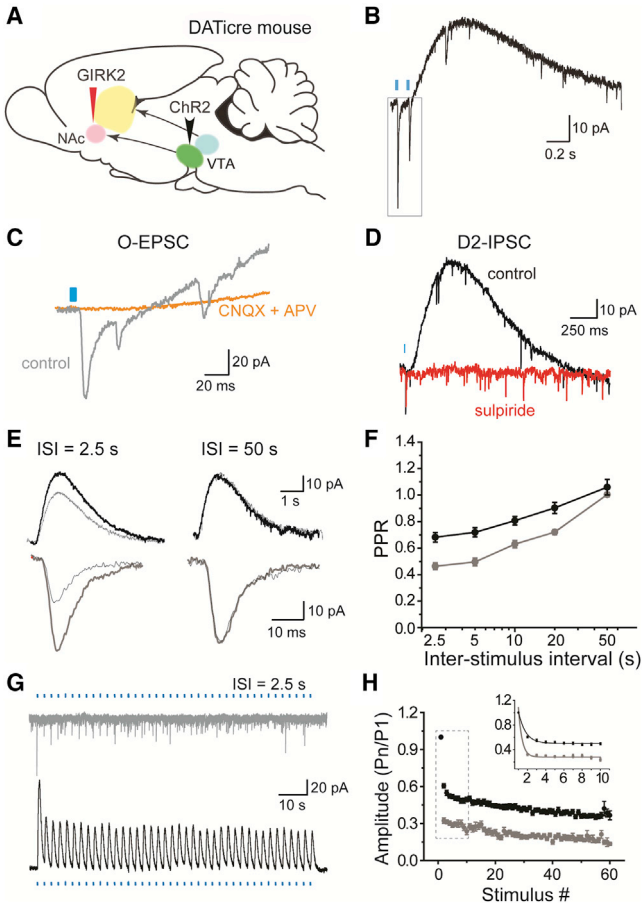

Figure 1. Glutamate and Dopamine Release by Dopamine Neurons Depress with Different Kinetics

(A) DATiCre$^{+/-}$ mice were injected with AAV2/9.hSyn.tdTomato.T2A.GIRK2.WPRE into the medial shell of the nucleus accumbens (NAc) and AAV5-EF1α-DIO-hChR2-mCherry into the VTA.

(B) Representative whole-cell recording from a GIRK2-expressing SPN shows light-evoked EPSC (O-EPSC) and D2 dopamine receptor-mediated inhibitory current (D2-IPSC) in response to successive stimulation with blue light at 0.4 Hz (blue bar).

(C) The AMPA receptor antagonist CNQX and NMDA receptor antagonist APV (orange) block the O-EPSC (gray).

(D) The D2 receptor antagonist sulpiride (1 μM, red) eliminates the D2-IPSC (black).

(E) Representative O-EPSC (gray) and D2-IPSC (black) responses to paired optogenetic stimulation at 2.5 and 50 s inter-stimulus intervals (ISI). The overlapping traces show two successive responses, with the first represented by a thick line and second by a thin line.

(F) Quantification of the paired-pulse response for O-EPSC (gray) and D2-IPSC (black) at different ISI. $p < 0.01$ by two-way ANOVA; n = 5–10 cells for each interval

(G) O-EPSCs and D2-IPSCs in response to repetitive optogenetic stimulation (60 pulses at 0.4 Hz).

(H) Summary of O-EPSC and D2-IPSC amplitude in response to repetitive stimulation at 0.4 Hz. Amplitudes were normalized to the first response in each recording. $p < 10^{-10}$ by one-way ANOVA; n = 19 cells for each.

Data in (F) and (H) indicate mean ± SEM. See also Figure S1.

d'Incamps et al., 2017; Ren et al., 2011; Sengupta et al., 2017) but convey the same information about neural activity. Ultrastructural analysis of the striatum has suggested segregation of dopamine and glutamate release sites (Zhang et al., 2015), but mesolimbic dopamine neurons appear to release glutamate and dopamine with very similar properties (Adrover et al., 2014). On the other hand, starburst amacrine cells in the retina corelease ACh and GABA, and their signaling shows a differential dependence on Ca^{2+}, suggesting a presynaptic mechanism for the differences in response (Lee et al., 2010). Recent work has suggested a similar difference between ACh and GABA release by basal forebrain neurons (Takács et al., 2018).

Previous work has attributed variation in the properties of release to extrinsic factors such as the association of synaptic vesicles with the cytoskeleton or their proximity to Ca^{2+} channels (Chi et al., 2001; Eggermann et al., 2011; Midorikawa et al., 2007). However, these and other extrinsic factors such as Ca^{2+} buffering cannot alone account for differences in the release of two transmitters by the same cell. Alternatively, synaptic vesicles may differ in their intrinsic properties, reflecting differences in composition and hence identity. The phenomenon of corelease provides an entry point to test this possibility.

RESULTS

Glutamate and Dopamine Release from VTA Dopamine Neurons Differ in Short-Term Plasticity

To assess the relationship between glutamate and dopamine release by ventral tegmental area (VTA) dopamine neurons, we used postsynaptic recording in brain slices. Since dopamine does not usually produce detectable postsynaptic currents, we took advantage of a G-protein-coupled inwardly rectifying K^+ channel (GIRK2) that couples to D2 dopamine receptors when expressed in striatal spiny projection neurons (SPNs) (Marcott et al., 2014), enabling direct comparison of postsynaptic glutamate and dopamine responses. After injection of recombinant AAV encoding GIRK2 into the ventral striatum, we expressed channelrhodopsin specifically in dopamine neurons by introducing the conditional AAV-EF1a-DIO-hChR2-mCherry into the VTA of mice expressing cre recombinase under the control of the dopamine transporter (DATicre). Using striatal slices from these mice, light evokes both rapid excitatory postsynaptic currents (EPSCs) and slow, inhibitory postsynaptic currents (IPSCs) in SPNs (Figures 1A and 1B). As expected, glutamate receptor antagonists 6-cyano-7-nitroquinoxaline-2,3-dione (CNQX) and 3-(2-carboxypiperazin-4-yl)propyl-1-phosphonic acid (APV) block the EPSC, and D2 dopamine receptor antagonist sulpiride completely abolishes the slow IPSC (Figures 1C and 1D). In addition, expression of GIRK2 was shown not to affect basic membrane properties, and the D2-IPSCs recorded here are smaller (in amplitude and duration) than those reported previously (Marcott et al., 2014).

The ability of vesicular glutamate transport to promote monoamine and ACh uptake requires storage of the two transmitters in at least some of the same synaptic vesicles (Gras et al., 2008; Hnasko et al., 2010; Nelson et al., 2014). Entry of the anion glutamate dissipates the lumen-positive membrane potential, thereby disinhibiting the H^+-ATPase to create the low internal pH that

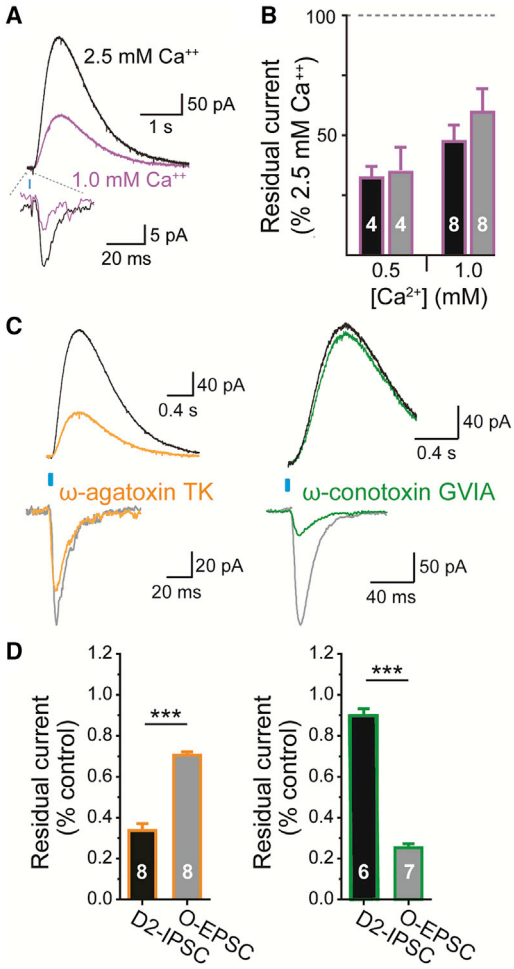

Figure 2. Glutamate and Dopamine Release by Dopamine Neurons Couple to Different Presynaptic Ca^{2+} Channels

(A) Representative recordings show O-EPSCs and D2-IPSCs in control (2.5 mM, black) and low (1.0 mM, purple) extracellular Ca^{2+}.

(B) Quantification of remaining current for the O-EPSC and D2-IPSC in 0.5 and 1.0 mM Ca^{2+}, relative to control (2.5 mM Ca^{2+}). The O-EPSC and D2-IPSC are reduced to a similar degree in both 0.5 and 1.0 mM Ca^{2+}. n = 4 for 0.5 mM Ca^{2+} and 8 for 1.0 mM Ca^{2+}

(C) Representative recordings show O-EPSCs and D2-IPSCs recorded in control, the P/Q-type Ca^{2+} channel blocker ω-agatoxin TK (300 nM, orange) or the N-type Ca^{2+} channel blocker ω-conotoxin GVIA (200 nM, green).

(D) Quantification shows the per cent residual O-EPSC and D2-IPSC in ω-agatoxin TK (orange) or ω-conotoxin GVIA (green) normalized to control without drug. ***p < 0.001 by Student's t test. n = 8 for ω-agatoxin TK, 6–7 for ω-conotoxin GVIA.

Data in (B) and (D) indicate mean ± SEM.

drives monoamine and ACh uptake. Since dissipation of the pH gradient can also create the membrane potential that drives glutamate transport (Goh et al., 2011) (Figure S1A) and vesicular monoamine transport involves H^+ exchange, we further assessed costorage by inhibiting VMAT2. As anticipated, the VMAT2 inhibitor tetrabenazine (TBZ; 5 μM) blocks the D2-IPSC, but it also reduces the amplitude of light-evoked EPSCs (Figures S1A and S1B). Uptake of dopamine by VMAT2 thus promotes glutamate storage and release, indicating at least some storage of both transmitters in the same vesicles. However, the extent of costorage remains unclear.

Although previous work has not indicated a difference in the release of glutamate and dopamine by mesolimbic dopamine neurons, dopamine release was measured by electrochemical detection with a carbon fiber electrode, which reflects dopamine spillover into the bulk extracellular space (Adrover et al., 2014). Taking advantage of GIRK2 expression to compare the postsynaptic responses to dopamine and glutamate, we observe a clear difference in paired pulse ratio (PPR) between the light-evoked D2-IPSC and the EPSC (Figures 1E and 1F). Due to the duration of the D2-IPSC, we stimulated at relatively long intervals (2.5–50 s). In slices, however, dopamine release exhibits long-lasting depression independent of D2 autoreceptors (Kennedy et al., 1992; Phillips et al., 2002; Shin et al., 2017) that enables us to compare the extent of depression even at this low stimulation frequency. The EPSC depresses more than the D2-IPSC and the difference is greatest at 2.5 s but remains throughout recovery (Figures 1E and 1F). In addition, prolonged stimulation at 0.4 Hz shows that the difference between D2-IPSC and EPSC persists throughout trains: the D2-IPSC remains easily detectable, whereas the EPSC almost disappears (Figures 1G and 1H). We used the D2 antagonist sulpiride to isolate the glutamate-mediated currents, but the blockade of autoreceptors does not affect the extent of depression at this low stimulation frequency (Benoit-Marand et al., 2001; Shin et al., 2017) (Figure S1C). We also blocked $GABA_A$, $GABA_B$, muscarinic, and D1 dopamine receptors, supporting direct rather than indirect, network effects of the transmitters released by dopamine neurons.

Use of GIRK channels to measure receptor activation has suggested that D2 dopamine receptors exhibit lower affinity than previously recognized (Marcott et al., 2014), but differences in receptor saturation might nonetheless account for the differences in synaptic depression between glutamate and dopamine. The amounts of dopamine released might decline as rapidly as the amounts of glutamate but show less apparent depression due to saturation of the first response. To assess this possibility, we reduced dopamine biosynthesis and stores by systemic injection of the tyrosine hydroxylase (TH) inhibitor α-methyl-p-tyrosine (AMPT). AMPT reduces the dopamine content in the nucleus accumbens (Figure S1D), indicating that the compound has reduced vesicular stores (Fon et al., 1997). In addition, AMPT slightly reduces EPSC amplitude (Figure S1E), as expected for the subset of synaptic vesicles storing both transmitters. However, AMPT has no effect on the synaptic depression observed with prolonged stimulation (Figure S1F), indicating that receptor saturation cannot account for the difference in depression from the EPSC.

The differences in short-term plasticity between glutamate and dopamine release by VTA dopamine neurons suggest a difference in sensitivity to Ca^{2+}. Relative to 2.5 mM external Ca^{2+}, however, optogenetic activation of mesostriatal terminals produces EPSCs and D2-IPSCs of similar magnitude in 0.5 and 1.0 mM Ca^{2+} (Figures 2A and 2B). Despite the lack of difference in Ca^{2+} sensitivity, we also tested the coupling to different Ca^{2+} channel subtypes. The P-/Q-type Ca^{2+} channel

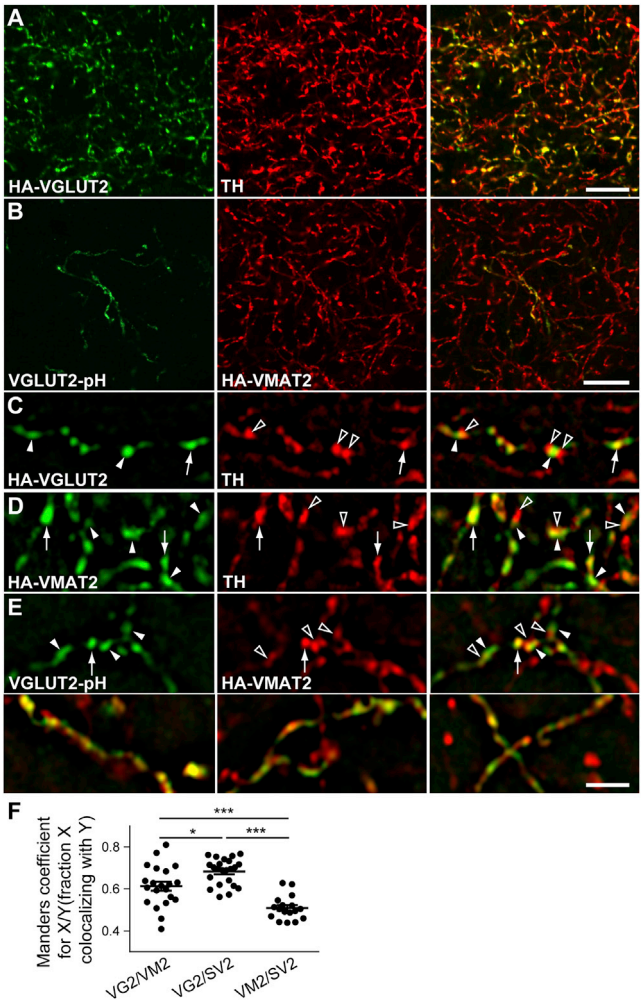

Figure 3. Epitope-Tagged VGLUT2 Expressed Specifically in DAT$^+$ Neurons Partially Colocalizes with Proteins Involved in Dopamine Release

(A–E) The ventral tegmental area (VTA) of DATicre (A and C) or DATicre;HA-VMAT2 BAC transgenic mice (B and E) was injected with recombinant AAV encoding cre-dependent HA-tagged VGLUT2 (AAV-DiO-HA-VGLUT2) (A and C) or cre-dependent pHluorin-tagged VGLUT2 (AAV-DiO-VGLUT2-pH) (B and E). Four weeks later, sections through the ventral striatum were double stained for HA and TH (A, C, and D) or GFP and HA (B and E).

(A) Representative confocal image of the ventral striatum from DATicre mice injected with AAV-DiO-HA-VGLUT2 and double stained for the conditional HA-VGLUT2 (green) and TH (red).

(B) Representative confocal image of DAT iCre;VMAT2-HA mice injected with AAV-DIO-VGLUT2-pHluorin and double stained for GFP and HA-VMAT2. Scale bars in (A) and (B) indicate 10 μm.

(C) Representative image acquired by structured illumination microscopy (SIM) of ventral striatum double stained for conditional HA-VGLUT2 and TH.

(D) SIM image of the ventral striatum from HA-VMAT2 BAC transgenic mice double stained for HA and TH. Filled arrowheads in (C) and (D) indicate HA immunoreactivity alone, open arrowheads TH alone and arrows double labeled punctae.

(E) Image of the ventral striatum from DATiCre, VMAT2-HA mice injected with AAV-DIO-VGLUT2-pHluorin double stained for GFP and HA-VMAT2. Filled arrowheads indicate GFP alone, open arrowheads HA alone, and arrows double labeling for both. Scale bar indicates 2 μm (C–E).

inhibitor ω-agatoxin TK inhibits the D2-IPSC more than the EPSC (Figures 2C and 2D). Remarkably, the N-type ω-conotoxin GVIA inhibits the EPSC much more strongly than the D2-IPSC (Figures 2C and 2D). Thus, glutamate release by dopamine neurons couples preferentially to N-type channels, and dopamine release to P-/Q-type channels (Phillips and Stamford, 2000), consistent with the storage of transmitter in different vesicle populations and perhaps release at distinct sites. Since these vesicle populations contain different transmitters, intrinsic differences in molecular composition must drive the differences in release.

Partial Segregation of VGLUT2 and VMAT2 within the Mesolimbic Dopamine Projection

The vesicular neurotransmitter transporters define the vesicles capable of exocytic release and can therefore be used to identify the sites of glutamate and dopamine storage. However, the striatum receives an extensive VGLUT2$^+$ projection from the thalamus (Härtig et al., 2003) in addition to the sparse VGLUT2 originating in midbrain dopamine neurons. Indeed, striatal VGLUT2 immunoreactivity shows remarkably little colocalization with TH (Figures S2A and S2D). VGLUT2 and TH have been suggested to segregate within the processes of dopamine neurons (Bérubé-Carriere et al., 2009; Kawano et al., 2006; Sulzer et al., 1998; Zhang et al., 2015), but VGLUT2 shows the same low colocalization with soluble fluorescent protein TdTomato expressed in dopamine neurons (Figure S2B), consistent with the predominant expression of striatal VGLUT2 by thalamic input.

To focus on the small proportion of striatal VGLUT2$^+$ processes made by midbrain dopamine neurons, we used adeno-associated virus (AAV) to express a cre-dependent allele of HA-tagged VGLUT2 (AAV-EF1a-DiO-VGLUT2-HA) specifically in the dopamine neurons of DATicre mice. Figure 3A shows that a large fraction of the processes expressing HA-VGLUT2 double label for TH. However, the higher resolution provided by structured illumination microscopy (SIM) (Schermelleh et al., 2008) reveals that HA-VGLUT2 segregates from TH at many but not all presynaptic sites (Figure 3C). Since the available VMAT2 antibodies are not sensitive or specific (Zhang et al., 2015), we also produced HA-VMAT2 BAC transgenic mice that show appropriate localization of the transgene in monoamine neurons and their projections (Figure S3). Like TH, HA-VMAT2 shows little colocalization with total VGLUT2 (Figure S2C). However, HA-VMAT2 also differs in localization from TH (Figure 3D) even though both proteins contribute to the release of dopamine. Presumably, synaptic vesicles (containing VMAT2) simply displace the soluble biosynthetic enzyme (Figures S2A and S2D). To compare localization of the two transporters, we therefore produced a recombinant AAV encoding a conditional allele of VGLUT2 fused to the ecliptic pHluorin, a modified form of GFP (VGLUT2-pH) (Foss et al., 2013). Injected into the VTA

(F) Colocalization was quantified by Manders coefficient (fraction X colocalizing with Y for X/Y = VGLUT2/VMAT2, VGLUT2/SV2, and VMAT2/SV2). *$p < 0.05$, ***$p < 0.001$ by one-way ANOVA with post hoc Bonferroni's test. In 3 mice, n = 21 fields for VGLUT2/VMAT2, 22 for VGLUT2/SV2, and 17 for VMAT2/SV2.

Data show the scatterplot and mean ± SEM. See also Figures S2 and S3.

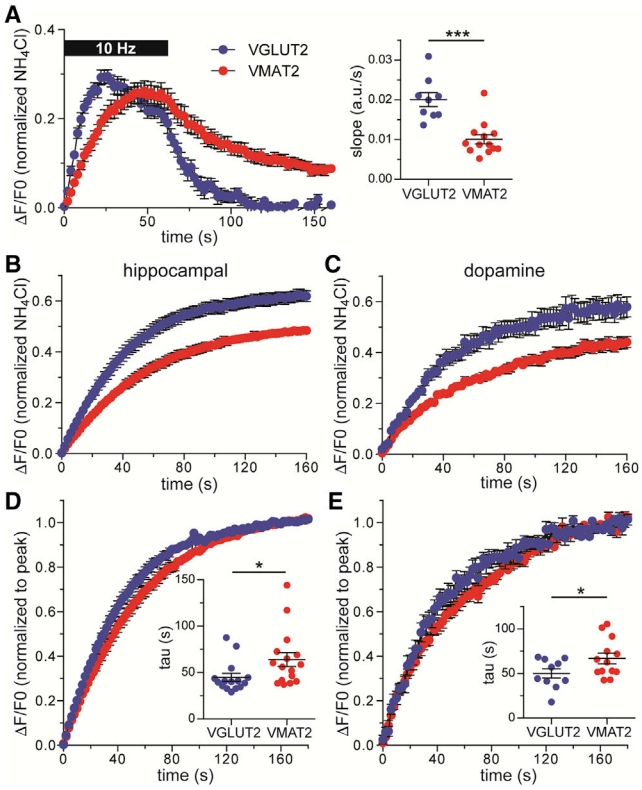

Figure 4. VGLUT2 and VMAT2 Differ in Response to Stimulation in Hippocampal as Well as Dopamine Neurons

(A) Mean response of VGLUT2-pHluorin (blue) and VMAT2-pHluorin (red) to 10 Hz stimulation for 60 s in hippocampal neurons from wild-type mice (left). The fluorescence is normalized to that observed after alkalinization in 50 mM NH_4Cl. The right panel shows the average initial slope for each coverslip. ***p = 0.0003 by Mann-Whitney test. n = 9 coverslips for VGLUT2 and 13 coverslips for VMAT2

(B and C) Mean response of VGLUT2- and VMAT2-pHluorin in hippocampal (B) and dopamine (C) neurons to 10 Hz stimulation for 3 min in 600 nM bafliomycin, normalized to fluorescence in NH_4Cl.

(D and E) Mean response of VGLUT2- and VMAT2-pHluorin to 10 Hz stimulation for 3 min in bafilomycin, normalized to the peak response at the end of stimulation in hippocampal (D) and dopamine (E) neurons. Insets show the quantification of exocytic time constant per coverslip.

Data indicate mean ± SEM n = 15 coverslips for VGLUT2 and 16 coverslips for VMAT2 in hippocampal neurons. *p = 0.0208 by Mann-Whitney test. n = 10 coverslips for VGLUT2 and 13 for VMAT2 in dopamine neurons. *p = 0.0453 by Student's t test.

of HA-VMAT2;DATicre mice, this construct colocalizes with HA-VMAT2 by standard confocal microscopy (Figure 3B). By SIM, however, HA-VMAT2 and GFP-VGLUT2 frequently segregate into adjacent but distinct punctae (Figure 3E). Quantitation confirms the reduced colocalization of VGLUT2 with VMAT2 relative to the canonical synaptic vesicle protein SV2 (Figure 3F). Consistent with this difference, SV2 colocalizes better with VGLUT2 than VMAT2 (Figure 3F). Since only dopamine neurons can express the epitope-tagged VGLUT2, these differences indicate that, despite overexpression, only a fraction of the introduced VGLUT2 colocalizes with VMAT2 (Hnasko et al., 2010), consistent with the difference between glutamate and dopamine release. At the sites where they colocalize, however, this analysis does not indicate whether the two transporters colocalize on the same vesicles.

Direct Imaging of VGLUT2 and VMAT2 Reveals Differences in the Kinetics of Exocytosis

Since differences in the properties or location of receptors might account for the observed differences in signaling by glutamate and dopamine, we sought direct evidence for differences in the regulated fusion of synaptic vesicles releasing the two transmitters. To identify the two vesicle populations, we took advantage of the ecliptic pHluorin, a pH-sensitive form of GFP, that we previously fused to the lumenal domains of VMAT2 and VGLUT2 (Foss et al., 2013; Onoa et al., 2010; Voglmaier et al., 2006). Quenched at the low pH of synaptic vesicles, the fluorescence of these fusion proteins increases with exposure to higher pH at exocytosis and then declines again after endocytosis, when the vesicle reacidifies (Miesenböck et al., 1998). We previously found that a substantially smaller fraction of VMAT2 resides on vesicles responsive to stimulation (recycling pool) than for other synaptic vesicle proteins including the VGLUTs, and the difference persisted in cultured hippocampal as well as midbrain dopamine neurons (Onoa et al., 2010). However, this may simply reflect the localization of VMAT2 to other membranes, such as endosomes, from which it cannot be mobilized by stimulation, rather than a difference in the kinetics of release by vesicles that do respond to stimulation.

To examine the kinetics of exocytosis, we introduced the pHluorin-tagged transporters by lentivirus into hippocampal and midbrain cultures, stimulating at 10 Hz for 60 s and normalizing the response to total reporter detected by alkalinization in NH_4Cl. In both hippocampal neurons and dopamine neurons (identified using the cre-dependent tdTomato reporter in midbrain cultures from DATicre mice), the fluorescence increases considerably faster for VGLUT2- than VMAT2-pHluorin (Figure 4A). Since endocytosis also occurs during stimulation, we used the H^+ pump inhibitor bafilomycin A1, which prevents vesicle reacidification and hence focuses on the delivery of new synaptic vesicles. Stimulating at 10 Hz for 3 min to empty the recycling pool, a larger proportion of VGLUT2 than of VMAT2 responds to stimulation in both hippocampal and dopamine neurons (Figures 4B and 4C), consistent with previous observations (Onoa et al., 2010). To determine whether the rates of release differ, we then normalized the fluorescence response to the peak at the end of stimulation. Even when normalized to peak response, VGLUT2-pHluorin responds more rapidly than VMAT2-pHluorin, again in both hippocampal and midbrain dopamine neurons (Figures 4D and 4E). Independent of recycling pool size, the imaging thus shows an intrinsic difference in the release rate of glutamate and monoamine vesicles, providing direct functional evidence for storage of the two transmitters in distinct vesicles, both of which respond to stimulation. The faster release of VGLUT2 than VMAT2 is consistent with the higher intrinsic release probability of glutamate predicted by the increased short-term depression of EPSCs relative to D2-IPSCs by slice physiology. Differences in behavior of the two transporters thus correspond to the differences in transmitter release.

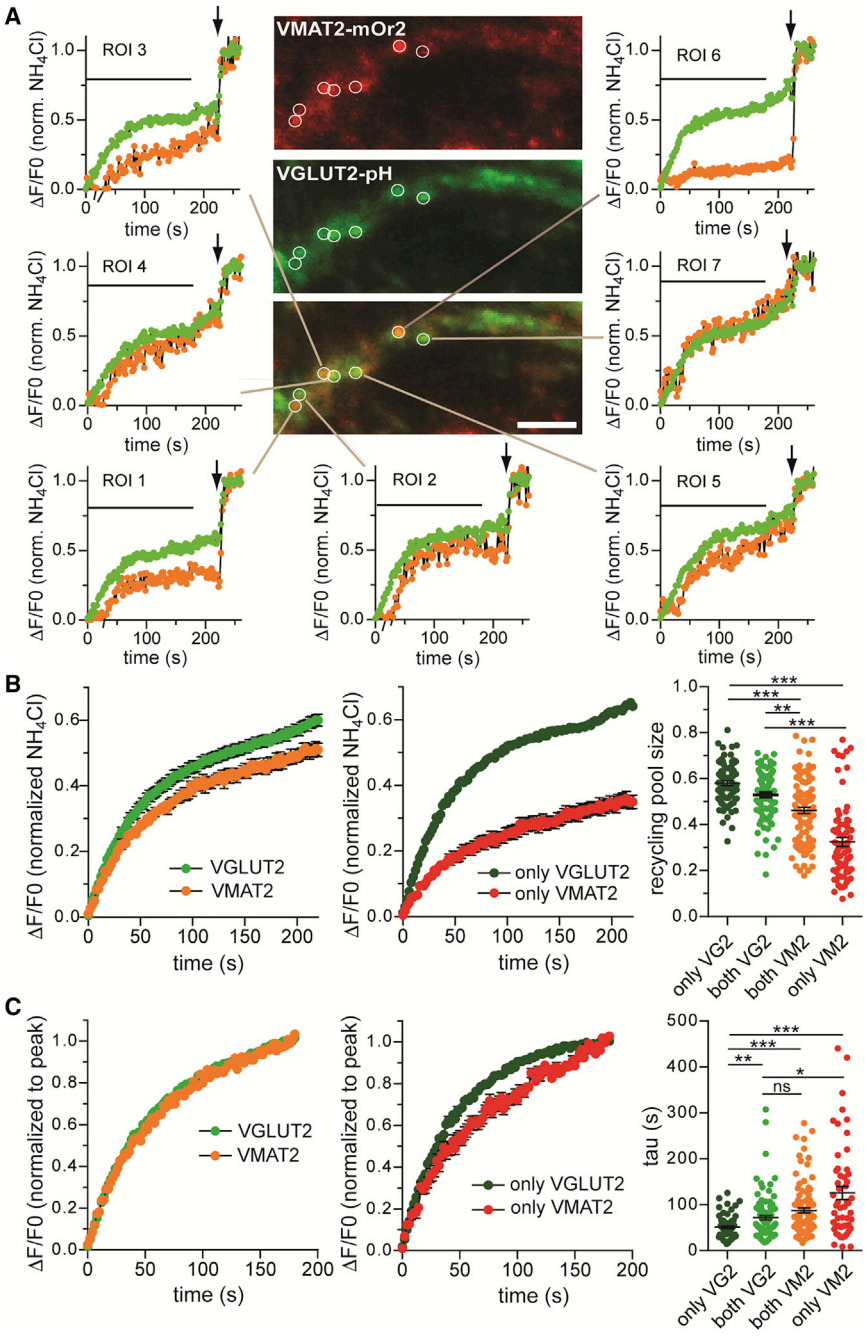

Figure 5. The Exocytosis of VGLUT2 and VMAT2 Differs at Individual Boutons

(A) Representative image from a hippocampal culture transduced with lentiviruses encoding VGLUT2-pHluorin (VGLUT2-pH, green) and VMAT2-mOrange2 (VMAT2-mOr2, red) and incubated in NH_4Cl (50 mM) to alkalinize acidic intracellular compartments. Circles indicate individual boutons expressing variable amounts of the two fluorescent proteins and corresponding curves the fluorescence response to 10 Hz stimulation for 3 min in bafilomycin (600 nM). Horizontal lines indicate 10 Hz stimulation, and the arrows indicate the addition of 50 mM NH_4Cl.

(B) VGLUT2-pH and VMAT2-mOr2 exhibit a similar recycling pool size when analyzed at boutons expressing both proteins but differ at boutons that express only one of the two fluorescent transporters ($p < 0.0001$ by Kruskal-Wallis one-way ANOVA with Dunn's post hoc test). $^{**}p < 0.01$; $^{***}p < 0.001$.

(C) Normalization to the peak response shows a similar rate of fluorescence increase for VGLUT2-pH and VMAT2-mOr2 at boutons expressing both proteins but an increased rate for VGLUT2 and a reduced rate for VMAT2 when comparing boutons that express only one of the transporters ($p < 0.0001$ by Kruskal-Wallis one-way ANOVA with Dunn's post hoc test). $^{**}p < 0.01$; $^{***}p < 0.001$.

Data in (B) and (C) indicate mean ± SEM n = 104 $VGLUT2^+/VMAT2^+$, 83 $VGLUT2^+$, and 75 $VMAT2^+$ boutons from 10 coverslips and 3 independent cultures. See also Figure S4.

Dual Imaging Reveals Bouton-Specific Properties of VGLUT2 and VMAT2 Exocytosis

Intrinsic differences in synaptic vesicles apparently drive variation in release but differences in location (Figure 3) (Zhang et al., 2015) may contribute to the expression of these differences. To address this possibility, we simultaneously imaged the behavior of both transporters. Replacing pHluorin in the lumenal loop of VMAT2 by the red-shifted pH-sensitive fluorescent protein mOrange2, we introduced this construct and VGLUT2-pHluorin by lentivirus, conferring expression in essentially all cells. For these experiments, we used hippocampal neurons because the mOr2 reporter precludes the use of tdTomato to identify midbrain dopamine neurons and because hippocampal neurons show the same difference between transporters as the dopamine neurons (Figure 4). Using NH_4Cl to reveal the total expression of each transporter (Figure 5A), we found a moderate correlation between VMAT2-mOr2 and VGLUT2-pHluorin (r = 0.54) (Figure S4A). However, many boutons express low levels of one reporter despite high levels of the other, and the data appear skewed toward a higher incidence of boutons with more VGLUT2 and less VMAT2, regardless of whether they were identified using GFP or mOr2 (data not shown). The two proteins can thus differ in location, consistent with distinct as well as overlapping release sites suggested by the analysis of dopamine projections *in vivo*.

We also used dual imaging to determine whether the differences in response reflect targeting of the two reporters to different vesicles at the same bouton. Focusing on boutons that express both reporters, we found that the proportion of VMAT2 responsive to stimulation varies considerably at different

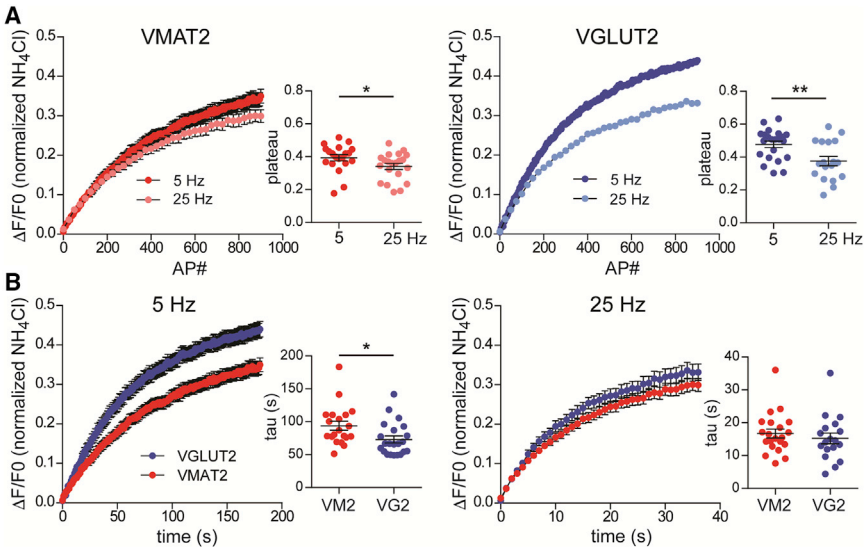

Figure 6. Exocytosis of VMAT2 and VGLUT2 Differ in Frequency Dependence

Dopamine neuron cultures from DATiCre/B6; 129S6-Gt(ROSA)26Sor$^{tm9(CAG-tdTomato)Hze}$/J mice were stimulated with 900 action potentials (APs) at either 5 or 25 Hz in the presence of bafilomycin, and the fluorescence normalized to that in the presence of NH_4Cl.

(A) Fitting the response to a single exponential, VMAT2-pH fluorescence reaches a slightly lower plateau after 900 AP stimulation at 25 Hz than after the same number of APs at 5 Hz (*p = 0.0294 by Mann-Whitney test). VGLUT2-pH reaches a substantially lower plateau at 25 Hz relative to 5 Hz (**p = 0.0044 by unpaired t test).

(B) Comparison of the two reporters stimulated at 5 Hz shows a faster response for VGLUT2-pH than VMAT2-pH (*p = 0.0437 by unpaired t test). At 25 Hz, the rate of response is similar for VGLUT2- and VMAT2-pH (p = 0.1643 by unpaired t test).

Data show mean ± SEM n = 22 coverslips for VGLUT2-pH at 5 Hz and 17 coverslips at 25 Hz; for VMAT2-pH, n = 20 coverslips for both 5 and 25 Hz stimulation. See also Figure S5.

boutons, in contrast to the typical synaptic vesicle protein VGLUT2, which responds more consistently (Figures 5A and S4B). Thus, the reporters must localize at least in part to different vesicles even when expressed at the same bouton. Surprisingly, VMAT2 responds to a lesser extent when total VMAT2 predominates and to a greater extent at boutons where total VGLUT2 predominates. The response of VMAT2 thus correlates with the expression of VGLUT2 and raises the possibility that VGLUT2 influences the trafficking of VMAT2.

We then assessed differences in the kinetics of release, normalizing to the maximum fluorescence after 10 Hz stimulation in bafilomycin. Despite the different rates of exocytosis observed when imaging the reporters individually (Figures 4D and 4E), Figure 5C shows that the average time constant of exocytosis does not differ between the two reporters imaged at the same boutons. Since co-localization with VGLUT2 may determine the properties of VMAT2, the differences observed by imaging the two reporters separately may reflect those boutons, which contain only one reporter.

Using alkalinization in NH_4Cl to identify boutons that contain only one of the two reporters, we first examined recycling pool size. Figure 5B shows that the difference between recycling pool size of VGLUT2 and VMAT2 differs much more dramatically when the transporters localize to distinct sites, and the increased difference derives from the reduced recycling pool size of VMAT2 when expressed alone, without VGLUT2. The kinetics of release also differ more dramatically at boutons containing only one reporter, in this case driven almost equally by increases in the rate of exocytosis by VGLUT2 and by decreases in VMAT2 (Figure 5C). Thus, targeting of the transporters to distinct release sites contributes to the differences in rate of release.

Glutamate and Dopamine Release Differ in Dependence on Stimulation Frequency

Previous work has shown that the slow Ca^{2+} chelator EGTA inhibits the response of VMAT2-pHluorin in dopamine neurons to a greater extent than the response of VGLUT1-pHluorin in hippocampal neurons (Pan and Ryan, 2012), indicating that the monoamine vesicles are more loosely coupled to presynaptic Ca^{2+} channels (Eggermann et al., 2011). This difference was attributed to the expression in dopamine neurons of the calcium-buffering protein calbindin (Pan and Ryan, 2012). However, the differential effect of conotoxins (Figure 2) now indicates that coupling to Ca^{2+} entry can differ among different synaptic vesicle populations within a single neuron. To assess the extent of coupling to presynaptic Ca^{2+} channels, we again used the pHluorin reporters expressed in hippocampal neurons, monitoring their sensitivity to the slow Ca^{2+} buffer EGTA, which limits the access of entering Ca^{2+} to more distant synaptic vesicles but not those directly adjacent to the site of Ca^{2+} entry. After loading with EGTA-AM (100 μM) or vehicle control, we examined the response of both reporters to brief, high-frequency stimulation (40 Hz for 2.5 s). Even in hippocampal neurons, EGTA inhibits the VMAT2 response to a greater extent than that of VGLUT2 (Figure S5A), again consistent with the lower probability of dopamine release predicted by paired pulse stimulation.

We also used the pHluorin reporters in bafilomycin to examine the frequency dependence of exocytosis by the different synaptic vesicle populations. Normalizing to stimulus number, VMAT2 shows little decrement at 25 Hz relative to 5 Hz (Figure 6A). In contrast, VGLUT2 shows a large decrement at 25 Hz, again consistent with vesicle depletion due to high release probability. Comparing the two transporters directly, VMAT2 shows less response than VGLUT2 at 5 Hz (Figure 6B), as predicted by the lower probability of dopamine release. At 25 Hz, however, the transporters show a similar response, consistent with the ability of VMAT2-containing synaptic vesicles to increase exocytosis with high-frequency stimulation and of dopamine signaling to encode frequency. Further, VMAT2 exhibits the same difference from VGLUT2 in hippocampal neurons, indicating that the mechanisms responsible are not restricted to dopamine neurons (Figure S5B).

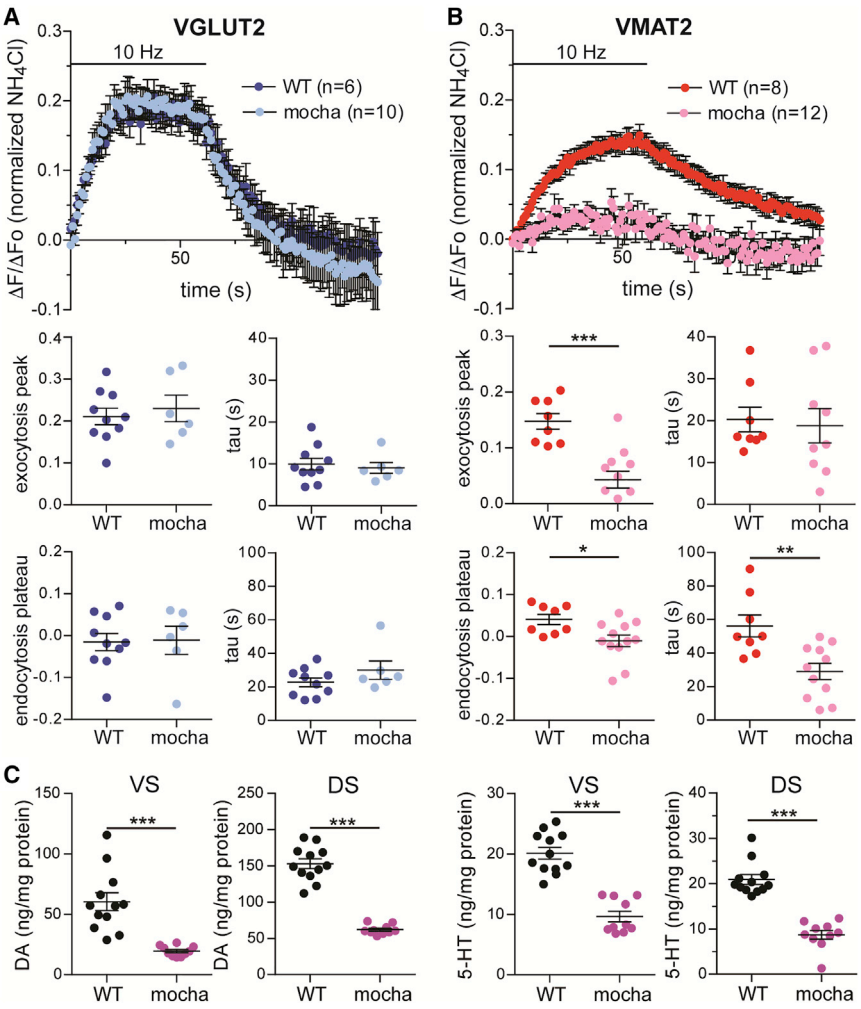

Figure 7. Loss of AP-3 Impairs the Response of VMAT2-pHluorin to Stimulation without Affecting VGLUT2-pHluorin

Dopamine neurons were identified using the fluorescent cocaine analog JHC 1–64 (30 nM), the cultures were stimulated at 10 Hz for 60 s, and the fluorescence was normalized to that observed after alkalinization in NH_4Cl.

(A) Mean response of VGLUT2-pH in dopamine neurons from wild-type (dark blue) and *mocha* mice (light blue). The rate of fluorescence increase ($p = 0.6676$ by unpaired t test) and peak fluorescence ($p = 0.5920$ by unpaired t test) during stimulation as well as the rate of fluorescence decline ($p = 0.4278$ by unpaired t test) and plateau ($p = 0.9136$ by unpaired t test) after stimulation shows no difference between wild-type and *mocha* neurons. Data indicate mean ± SEM n = 10 coverslips for wild-type and 6 coverslips for *mocha* neurons

(B) Mean response of VMAT2-pH in dopamine neurons from wild-type (red) and *mocha* mice (pink). The peak fluorescence response shows a substantial reduction in *mocha* neurons relative to wild type (***$p = 0.0001$ by unpaired t test), whereas exocytosis kinetics do not differ ($p = 0.7747$ by unpaired t test). Compensatory endocytosis reaches a lower plateau (*$p = 0.0180$ by unpaired t test) with faster kinetics (**$p = 0.0032$ by unpaired t test) in neurons from *mocha* mice relative to wild type. Data indicate mean ± SEM n = 8 coverslips for wild-type and 12 coverslips for *mocha* neurons

(C) The *mocha* mutation greatly reduces dopamine (DA) and serotonin (5-HT) levels in the ventral striatum (VS) and dorsal striatum (DS). ***$p < 0.001$ by unpaired t test. n = 12 for WT and 10 for *mocha*. See also Figure S6.

Synaptic Vesicles Releasing Glutamate and Dopamine Form through Different Recycling Pathways

The differences in neurotransmitter content and release properties indicate that synaptic vesicles containing glutamate and dopamine differ in identity, predicting that they also differ in biogenesis. Although synaptic vesicles generally form through a clathrin-dependent mechanism that involves the heterotetrameric adaptor protein AP-2 (Kononenko et al., 2014; Saheki and De Camilli, 2012; Watanabe et al., 2014), specific proteins such as the zinc transporter ZnT3 and v-SNARE VAMP7 require the related adaptor AP-3 for targeting to synaptic vesicles (Salazar et al., 2004; Scheuber et al., 2006). Loss of AP-3 in *mocha* mice has little effect on synaptic transmission but does impair asynchronous release at hippocampal mossy fiber synapses (Evstratova et al., 2014). Thus, we considered the possibility that AP-3 contributes to the formation of specific synaptic vesicles that might also differ in neurotransmitter content. To test this, we imaged the behavior of VGLUT2- and VMAT2-pHluorin in dopamine neurons from wild-type and *mocha* mice. As predicted from the modest effects on excitatory transmission (Evstratova et al., 2014; Voglmaier et al., 2006), VGLUT2-pHluorin responds to stimulation and undergoes compensatory endocytosis with the same kinetics in both wild-type and *mocha* neurons (Figure 7A). However, the *mocha* mutation greatly reduces the response of VMAT2-pHluorin to stimulation (Figure 7B). Considering the role of AP-3 in synaptic vesicle formation, the requirement for AP-3 of VMAT2 but not VGLUT2 suggests that AP-3 specifically contributes to the formation of vesicles that store dopamine, not glutamate. The rate and extent of compensatory endocytosis also appears enhanced by the *mocha* mutation, suggesting redistribution of the transporter to a different recycling pathway in the absence of AP-3.

In addition to the defect in VMAT2 exocytosis, imaging of the pHluorin reporter showed a major reduction in total presynaptic VMAT2 assessed by unquenching of the intracellular protein in NH_4Cl (1,436 ± 71 a.u., n = 120 boutons for wild type [WT] versus 753 ± 33 a.u., n = 165 boutons for *mocha*, $p < 0.0001$ by Mann-Whitney). In contrast, VGLUT2-pHluorin showed no difference between *mocha* and WT (750 ± 40 a.u., n = 131 boutons for WT versus 672 ± 35 a.u., n = 90 boutons for *mocha*, $p = 0.343$ by Mann-Whitney). This suggested an additional defect in axonal targeting of specifically VMAT2 that should affect the vesicular

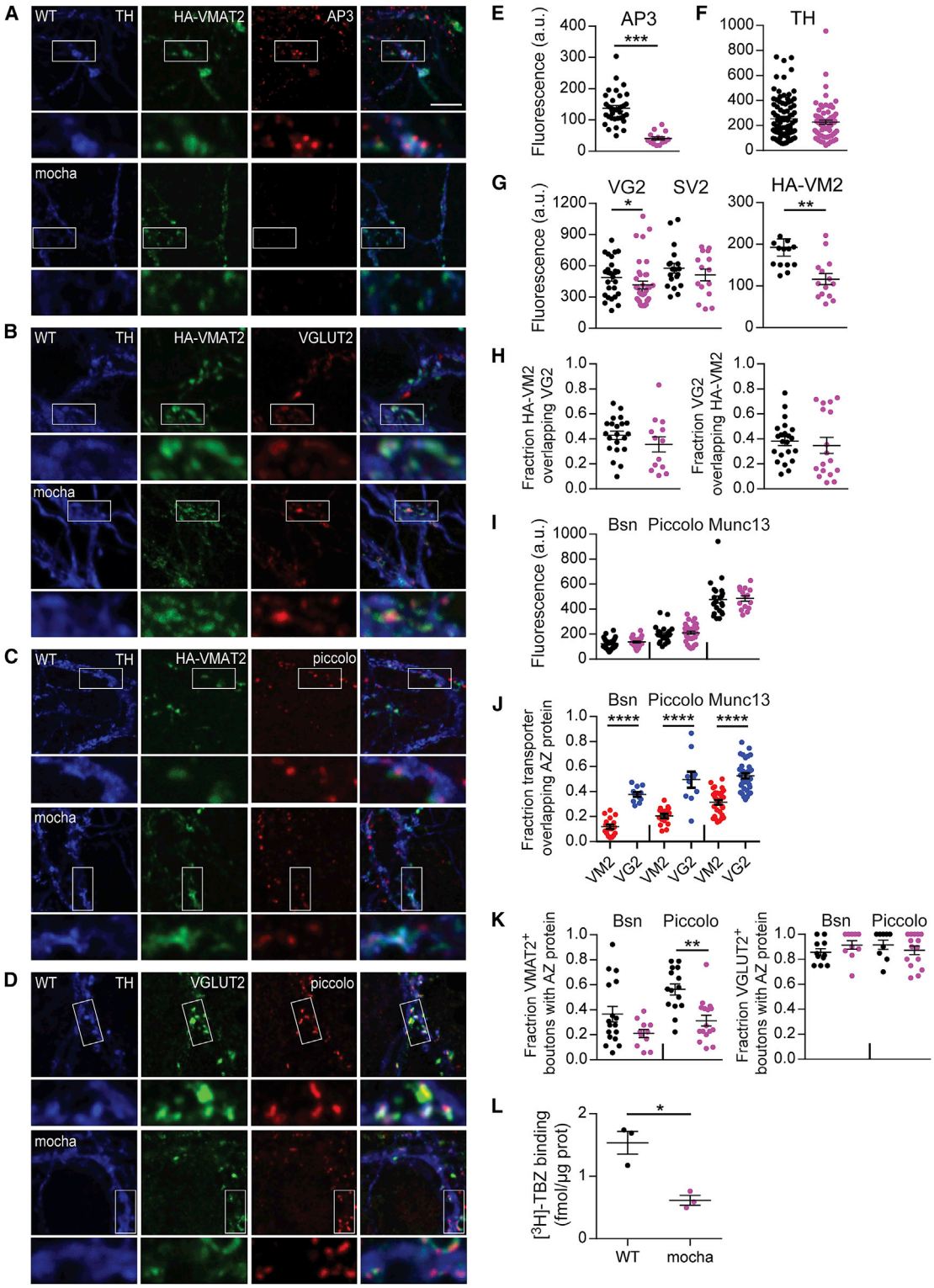

Figure 8. Loss of AP3 Reduces VMAT2 Localization to Dopamine Neuron Release Sites

(A–D) Confocal images of midbrain cultures from HA-VMAT2/WT mice (top) and HA-VMAT2/*mocha* mice (bottom).

(A) TH^+ neurons label for AP-3 in WT but not *mocha* cultures (quantified in E).

(B) VGLUT2 and VMAT2 colocalize in a subset of TH^+ boutons in both wild-type and *mocha* cultures (quantified in H).

(legend continued on next page)

stores of dopamine. To test this possibility *in vivo*, we measured the tissue content of monoamine, which reflects vesicular stores (Fon et al., 1997; Takahashi et al., 1997; Wang et al., 1997). Figure 7C shows that the *mocha* mutation greatly reduces tissue dopamine and serotonin content in both regions. However, the metabolites of dopamine and serotonin both show either less or no reduction in the absence of AP-3 (Figure S6). The metabolite/monoamine ratio thus suggests increased monoamine turnover in *mocha* mice. Since the pHluorin imaging and catecholamine levels suggest reduced presynaptic localization of VMAT2 in *mocha* neurons, we also measured the binding of specific VMAT2 ligand [^{3}H]-tetrabenazine to striatal homogenates, observing an ~50% reduction in *mocha* tissue relative to WT (Figure 8L). Thus, *mocha* mice show impaired axonal targeting of VMAT2 *in vivo*.

To characterize the role of AP-3 in the structure of release sites formed by dopamine neurons, we prepared midbrain cultures from HA-VMAT2 BAC transgenic mice with and without the *mocha* mutation. Figures 8A and 8E show that AP-3 colocalizes with VMAT2 at TH$^+$ boutons, and *mocha* neurons do not label for AP-3, indicating antibody specificity. The *mocha* mutation reduces expression of HA-VMAT2 more significantly than that of VGLUT2 and does not affect labeling for SV2, consistent with a more important role for AP-3 in dopamine release (Figures 8A, 8F, and 8G). Despite the reduction in transporter labeling, the extent of colocalization remains unaffected by the loss of AP-3, although the extent of colocalization varies greatly among cells (Figures 8B and 8H).

To determine whether the effect of *mocha* on release reflects a change in the localization of VMAT2$^+$ and VGLUT2$^+$ vesicles to the active zone, we stained for active zone proteins bassoon, piccolo, and munc13. Loss of AP-3 does not affect the average fluorescence intensity of TH$^+$ punctae that label for these proteins (Figures 8C, 8D, and 8I). Consistent with recent work that indicates synaptic signaling by dopamine at active zones (Liu et al., 2018; Marcott et al., 2014), VMAT2 colocalizes with all three active zone proteins. However, VGLUT2 colocalizes with them to a greater extent than VMAT2 (Figures 8C, 8D, and 8J), supporting a more synaptic mode of signaling by glutamate. Indeed, almost all VGLUT2$^+$ boutons contain active zone proteins, and this proportion is unaffected by the *mocha* mutation. In contrast, a much smaller proportion of VMAT2$^+$ boutons label for an active zone protein, and the *mocha* mutation selectively reduces the fraction of boutons colocalizing with piccolo, not bassoon (Figures 8C, 8D, and 8K). Thus, loss of AP-3 does not disrupt presynaptic architecture. Rather, it selectively influences monoamine release sites, and the reduced colocalization with piccolo presumably reflects the disturbance in monoamine vesicles.

DISCUSSION

The results show that dopamine neurons release glutamate and dopamine from synaptic vesicles with different functional properties. The rates of synaptic depression observed for the two transmitters in striatal slices strongly suggest a presynaptic locus for the differences in signaling, and dependence on different presynaptic Ca^{2+} channels further supports a difference in release. Taking advantage of the vesicular transporters to label the two vesicle populations, imaging in culture provides direct evidence for differences in their behavior. The slower response of VMAT2 than VGLUT2 is consistent with the low release probability inferred from slice recording. Increased sensitivity to EGTA supports the looser coupling of VMAT2$^+$ vesicles to presynaptic Ca^{2+} channels. On the other hand, the effect of glutamate on dopamine (and ACh) storage (Gras et al., 2008; Hnasko et al., 2010; Nelson et al., 2014; Tritsch et al., 2012) and here of dopamine on glutamate storage suggest that a subpopulation of synaptic vesicles store both transmitters. Although the transporters frequently differ in localization, they can therefore occur on the same vesicles.

(C) Piccolo colocalizes with VMAT2 in a subset of TH$^+$ boutons in both WT and *mocha* cultures. The *mocha* mutation reduces the colocalization of piccolo and VMAT2 (quantified in K).

(D) Piccolo colocalizes with VGLUT2 in a subset of TH$^+$ boutons from wild-type and *mocha* mice (quantified in K). Outlined areas are magnified below. Scale bar, 5 μm.

(E–K) Quantitation of the results shown in (A)–(D), with WT in black and *mocha* in magenta.

(E and F) The *mocha* mutation eliminates immunolabeling for AP3 ($p < 0.0001$ by Mann-Whitney) (E) (n = 34 images for WT and 16 images for *mocha* from 3 coverslips of each) and does not affect immunofluorescence intensity for TH ($p = 0.4756$ by Mann-Whitney) (F) (n = 90 images for WT and 79 images for *mocha* from 9 coverslips of each).

(G) The boutons of *mocha* neurons show reduced labeling intensity for both VGLUT2 and VMAT2 but not SV2. $p = 0.0227$ by Mann-Whitney for VGLUT2 (n = 38 for WT and 47 for *mocha* from 6 coverslips of each), $p = 0.0017$ by Mann-Whitney for VMAT2 (n = 13 images for WT and 14 for *mocha* from 3 coverslips of each), and $p = 0.3865$ by Mann-Whitney for SV2 (n = 18 images for WT and 15 for *mocha* from three coverslips of each).

(H) Colocalization in TH$^+$ neurons of VGLUT2 and HA-VMAT2 (Manders coefficients) is unaffected by the loss of AP3. $p = 0.1555$ by unpaired t test for HA-VMAT2/VGLUT2 (left) and $p = 0.7220$ by Mann-Whitney for VGLUT2/HA-VMAT2 (right). n = 22 images for WT and 15 for *mocha.*

(I) The intensity of labeling for active zone proteins bassoon (Bsn), piccolo, and munc13 is unaffected by the *mocha* mutation. $p = 0.1094$ for bassoon (n = 35 images for WT and 27 for *mocha* from 3 coverslips of each), $p = 0.3369$ for piccolo (n = 23 images for WT and 35 for *mocha* from 3 coverslips of each), and $p = 0.2759$ for munc13 (n = 23 images for WT and 15 for *mocha* from 3 coverslips of each), all by unpaired t test.

(J) VGLUT2$^+$ punctae show greater colocalization than HA-VMAT2$^+$ punctae with active zone proteins bassoon, piccolo, and munc13. $p < 0.0001$ by unpaired t test for bassoon, piccolo, and munc13. n = 17 images for bassoon/VM2, 11 for bassoon/VG2, 16 for piccolo/VM2, 10 for piccolo/VG2, 31 for munc13/VM2, and 35 for munc13/VG2.

(K) The *mocha* mutation reduces the fraction of VMAT2$^+$ boutons colocalizing with piccolo ($p = 0.0004$, n = 15 images for WT, 16 for *mocha*) but not bassoon ($p = 0.1454$, n = 17 images for WT, 11 for *mocha*) or the fraction of VGLUT2$^+$ boutons with either active zone protein ($p = 0.1386$ for VGLUT2/bassoon, n = 11 images for WT and 10 for *mocha* and $p = 0.3983$ for VGLUT2/piccolo (n = 9 images for WT and 15 for *mocha)*, all by unpaired t test.

(L) Specific [^{3}H]-tetrabenazine binding is severely reduced in the striatal homogenates of *mocha* mice relative to WT (*$p < 0.05$ by two-way ANOVA). n = 3 mice/genotype.

Scatterplots show mean ± SEM. *$p < 0.05$; **$p < 0.01$; ***$p < 0.001$; ****$p < 0.0001$.

Previous work has shown that differences in the properties of transmitter release reflect differences in the association of synaptic vesicles with the cytoskeleton, synaptic ribbons, and coupling to presynaptic Ca^{2+} channels (Chi et al., 2001; Eggermann et al., 2011; Midorikawa et al., 2007). However, the demonstration that synaptic vesicles differ in transmitter content, and content correlates with the properties of release, means that differences in vesicle identity drive the differences in release and may indeed dictate the differences in cytoskeletal association and localization. Further, the selective effect of the *mocha* mutation on trafficking of VMAT2 demonstrates that monoamine vesicles require a recycling pathway that involves AP-3 in addition to (or perhaps instead of) the canonical clathrin adaptor AP-2, which regenerates most synaptic vesicles (Kononenko et al., 2014; Saheki and De Camilli, 2012; Watanabe et al., 2014). We infer that the pathway of recycling generates synaptic vesicles with different release properties, suggesting a previously unrecognized linkage between specific endocytic and exocytic limbs of the synaptic vesicle cycle.

A previous report has suggested that midbrain dopamine neurons form entirely distinct release sites for glutamate and dopamine (Zhang et al., 2015). The analysis by super-resolution microscopy now shows that the two sites are usually adjacent. The apparent discrepancy may reflect the difference in resolution between light and electron microscopy, but we have also found that the most strongly $VGLUT2^{+}$ striatal boutons derive from the thalamic projection. Expression of a conditional, epitope-tagged VGLUT2 was thus required to identify the VGLUT2 in dopaminergic boutons. Despite overexpression of VGLUT2, we observe partial segregation of the two vesicle populations. Immunoisolation has also been used to assess the colocalization of VMAT2 and VGLUT2 on striatal synaptic vesicles, showing either some or no colocalization (Hnasko et al., 2010; Zhang et al., 2015). However, the inefficiency of immunoisolation together with the expression of VGLUT2 by abundant thalamic inputs that do not express VMAT2 and the expression of VGLUT2 by only a subset of dopamine inputs make it difficult to draw conclusions from these data about segregation of the two transporters *within* dopamine neurons.

Why did voltammetry not detect a difference in release of glutamate and dopamine (Adrover et al., 2014)? Voltammetry measures dopamine overflow out of the synapse, and clearance by the dopamine transporter may underestimate the extent of release, increasing the apparent depression to resemble that observed for EPSCs. In contrast, the D2-IPSC measures the direct postsynaptic response. Previous work has suggested that dopamine release depends more on N-type Ca^{2+} channels (Brimblecombe et al., 2015; Phillips and Stamford, 2000), but this may also reflect the measurement of overflow by voltammetry.

The differences in release of glutamate and dopamine provide a physiological rationale for different synaptic vesicle recycling pathways. AP-3 regenerates synaptic vesicles from endosomes (Blumstein et al., 2001; Faúndez et al., 1997, 1998) and appears required for the localization of particular proteins to synaptic vesicles (Kantheti et al., 1998; Newell-Litwa et al., 2010; Scheuber et al., 2006). However, *mocha* mice lacking AP-3 form synapses with relatively normal excitatory transmission (Evstratova et al., 2014; Martinez-Arca et al., 2000; Voglmaier et al., 2006). The preferential effect of AP-3 loss on VMAT2 rather than VGLUT2 now provides an explanation for the modest effects previously reported—AP-3 is required specifically for the release of dopamine, not glutamate. Since VMAT2 transports norepinephrine and serotonin, we presume that this mechanism contributes to the regulated release of all monoamine transmitters. Consistent with a role for AP-3 in the recycling of monoamine synaptic vesicles, we find that the adaptor localizes to presynaptic boutons. The known role of AP-3 at endosomes further suggests that VMAT2 recycles through this compartment rather than directly from the plasma membrane.

However, loss of AP-3 also appears to reduce the axonal localization of VMAT2. *Mocha* mice show a large depletion of striatal monoamine content, which reflects vesicular stores and/or the activity of VMAT2. Live imaging of VMAT2-pHluorin in the presence of NH_4Cl shows a reduction in total presynaptic VMAT2 in *mocha* neurons. Immunofluorescence for HA-VMAT2 confirms the reduction *in vitro*, and the effect of the *mocha* mutation on VGLUT2 is less significant, supporting the specificity suggested by live imaging. Further, striatal homogenates from *mocha* mice show greatly reduced binding to the VMAT2 ligand ^{3}H-tetrabenazine. These results indicate a role for AP-3 in axonal targeting of VMAT2, in addition to its local, presynaptic role in vesicle recycling. Interestingly, AP-3 is required for presynaptic differentiation in *C. elegans* (Li et al., 2016), and the reduced axonal targeting of VMAT2 in *mocha* mice presumably reflects this ancestral role in neuronal polarity.

Previously, we found that AP-3 also sorts VMAT2 to peptidergic large dense core vesicles (LDCVs) (Asensio et al., 2010; Sirkis et al., 2013). Since LDCVs can deliver membrane proteins to the cell surface where they recycle into synaptic vesicles (Strasser et al., 1999), the axonal targeting of VMAT2 may involve LDCVs. The exocytosis of LDCVs also requires strong stimulation due to their distance from the sites of Ca^{2+} entry, raising the possibility that localization to LDCVs accounts for the differences in release from glutamate. However, imaging of LDCV exocytosis with peptide-pHluorin reporters, in neurons as well as endocrine cells, shows sudden, discrete increases in fluorescence sparsely distributed throughout the axon (Logan et al., 2017; van de Bospoort et al., 2012), very different from the general, graded increase in synaptic fluorescence reported here for VMAT2-pHluorin. Despite repeated attempts, we have rarely observed abrupt, focal exocytosis of VMAT2-pHluorin in neurons (unpublished observations). In addition, although VMAT2 localizes to LDCVs in endocrine cells, the transporter targets strongly to synaptic vesicles in neurons (Zhang et al., 2015), and dopamine neurons contain very few LDCVs (Nirenberg et al., 1997, 1998). Thus, release from LDCVs cannot account for the properties of VMAT2-pHluorin reliably elicited by stimulation in neurons.

The difference in release probability for $VGLUT2^{+}$ and $VMAT2^{+}$ vesicles, together with the differences in coupling to presynaptic Ca channels, suggests that the two vesicle populations may also differ in their targeting to the presynaptic active zone. Indeed, VGLUT2 colocalizes to a greater extent than VMAT2 with bassoon, piccolo, and munc13. Consistent with recent evidence for synaptic signaling by dopamine (Liu et al., 2018; Marcott et al., 2014), a substantial fraction of $VMAT2^{+}$ boutons

nonetheless contain all three active zone proteins. Interestingly, loss of AP-3 specifically reduces the presence of piccolo at VMAT2$^+$ boutons, with no effect on bassoon or expression of either active zone protein at VGLUT2$^+$ boutons. The trafficking mediated by AP-3 thus influences specific features of the active zone but only at VMAT2$^+$ boutons, consistent with its role in trafficking of this transporter and presumably other proteins that recycle through the same pathway.

The results also show that VGLUT2 and VMAT2 respond differently to stimulation in hippocampal as well as midbrain dopamine neurons. This suggests the transporters target to synaptic vesicle populations that exist in many neuronal populations. In hippocampal neurons, loss of AP-3 indeed impairs asynchronous glutamate release (Evstratova et al., 2014). Thus, AP-3 may target VMAT2 to synaptic vesicles that confer asynchronous release, consistent with weak coupling to presynaptic Ca^{2+} channels. VGLUT2 sorts to synaptic vesicles that couple more tightly, and VGLUT recycling depends primarily on the clathrin adaptor AP-2 (Foss et al., 2013; Kim and Ryan, 2009). However, other adaptors such as AP-3 may target the VGLUTs to vesicles with low release probability, conferring the observed asynchronous release (Evstratova et al., 2014; Li et al., 2017; Salazar et al., 2005).

Dual imaging of VGLUT2 and VMAT2 shows that exocytosis of the two vesicle populations can differ considerably at individual boutons, supporting the segregation to distinct vesicles even when they colocalize by light microscopy. Indeed, recent work on the corelease of GABA by cholinergic basal forebrain neurons has shown differences in release of these two transmitters despite storage at the same release site by electron microscopy (Takács et al., 2018). The segregation of release sites in dopamine neurons suggests differences from basal forebrain neurons, and we find differences in recycling pool size and exocytosis kinetics for VMAT2 and VGLUT2 are larger when comparing sites that contain only one of the two transporters. Although vesicle identity appears to drive the differences in release, the release site thus contributes to these differences, due to the expression of different Ca^{2+} channels or different recycling pathways. Recent work has suggested that dopamine neurons exhibit a high probability of dopamine release due to the expression of active zone components (Liu et al., 2018). Indeed, dopamine release shows prolonged short-term depression by D2-IPSC as well as voltammetry. Nonetheless, the probability of dopamine release is lower than that of glutamate release by the same cells, which may reflect association with different active zone components. Postsynaptic target neurons in the striatum may contribute to the segregation of release sites (Fortin et al., 2019), but we observe differential release in the absence of these cells, and it is possible that the transporters themselves also contribute. Indeed, VMAT2 belongs to the same family as the vesicular ACh transporter, but ACh release from basal forebrain neurons depends more on N-type channels (Takács et al., 2018), in contrast to dopamine release from midbrain neurons, which depends on P/Q-type. On the other hand, VGLUT1 has been shown to influence the endocytosis of other synaptic vesicle proteins (Pan et al., 2015), raising the possibility that the transporters influence vesicle composition and, as a result, exocytosis.

The morphological homogeneity of synaptic vesicles (Peters et al., 1970) has suggested that they use a common final pathway to regulated exocytosis, with variation due to extrinsic factors that influence their mobilization (Kim and Ryan, 2010), rather than intrinsic differences in their composition (Alabi and Tsien, 2012; Rizzoli and Betz, 2005). Recent work has suggested that synaptic vesicles undergoing spontaneous release belong to a distinct pool that does not respond to stimulation (Ramirez and Kavalali, 2011; Sara et al., 2005), although this has been controversial (Bal et al., 2013; Fredj and Burrone, 2009; Groemer and Klingauf, 2007; Hua et al., 2010, 2011; Ramirez et al., 2012). We now provide functional evidence for intrinsic differences in synaptic vesicle composition (neurotransmitter content) within the pool that does respond to stimulation. AP-3 produces a biochemically distinct set of synaptic vesicles with lower release probability and reduced synchrony due at least in part to differences in coupling to presynaptic Ca^{2+} channels. Corelease takes advantage of these general endocytic mechanisms to store transmitter in vesicle populations with different release properties and so deconvolve neural activity into two outputs, with distinct physiological and behavioral roles.

STAR★METHODS

Detailed methods are provided in the online version of this paper and include the following:

- KEY RESOURCES TABLE
- CONTACT FOR REAGENT AND RESOURCE SHARING
- EXPERIMENTAL MODEL AND SUBJECT DETAILS
  - Mice
  - Generation of HA-VMAT2 BAC transgenic mice
  - Primary culture
- METHOD DETAILS
  - Stereotactic virus injection
  - Immunohistochemistry
  - Slice electrophysiology
  - Measurement of monoamine levels
  - [^{3}H]-Dihydrotetrabenazine binding
  - Live imaging
- QUANTIFICATION AND STATISTICAL ANALYSIS
  - Data analysis
  - Statistics
- DATA AND SOFTWARE AVAILABILITY

SUPPLEMENTAL INFORMATION

Supplemental Information can be found online at https://doi.org/10.1016/j.neuron.2019.03.031.

ACKNOWLEDGMENTS

We thank members of the Edwards lab for helpful discussion, the lab of Anatol Kreitzer for guidance in the recording from striatal slices, DeLaine Larsen for assistance with the structured illumination microscopy, Susan Voglmaier for constructs, and Barry Calagui and Samir Batarni for technical support. This work was supported by a fellowship from the Fondation Fyssen and support from the Feldman Foundation (to K.S.), F30 DA40996 (to P.F.M.), R01 DA35821 and NS95809 (to C.P.F.), P01 DA10154 (to R.H.E.), the UCSF Kavli

Institute for Fundamental Neuroscience, and the UCSF Weill Institute for Neurosciences.

AUTHOR CONTRIBUTIONS

K.S., J.Y., and R.H.E. conceived of these experiments. K.S. performed both the immunofluorescence in striatal slices and the live imaging of midbrain dopamine and hippocampal neurons. C.S.A. produced the HA-VMAT2 BAC transgenic mice. J.Y. and P.F.M. performed the slice physiology with guidance from C.P.F. J.E. measured tetrabenazine binding. D.A.G. and A.H.N. synthesized JHC1-64. R.H.E. oversaw the project and together with K.S. and J.Y. assembled the manuscript.

DECLARATION OF INTERESTS

The authors declare no competing interests.

Received: May 14, 2018
Revised: January 28, 2019
Accepted: March 19, 2019
Published: April 16, 2019

REFERENCES

Adrover, M.F., Shin, J.H., and Alvarez, V.A. (2014). Glutamate and dopamine transmission from midbrain dopamine neurons share similar release properties but are differentially affected by cocaine. J. Neurosci. *34*, 3183–3192.

Alabi, A.A., and Tsien, R.W. (2012). Synaptic vesicle pools and dynamics. Cold Spring Harb. Perspect. Biol. *4*, a013680.

Asensio, C.S., Sirkis, D.W., and Edwards, R.H. (2010). RNAi screen identifies a role for adaptor protein AP-3 in sorting to the regulated secretory pathway. J. Cell Biol. *191*, 1173–1187.

Bal, M., Leitz, J., Reese, A.L., Ramirez, D.M., Durakoglugil, M., Herz, J., Monteggia, L.M., and Kavalali, E.T. (2013). Reelin mobilizes a VAMP7-dependent synaptic vesicle pool and selectively augments spontaneous neurotransmission. Neuron *80*, 934–946.

Benoit-Marand, M., Borrelli, E., and Gonon, F. (2001). Inhibition of dopamine release via presynaptic D2 receptors: time course and functional characteristics in vivo. J. Neurosci. *21*, 9134–9141.

Bérubé-Carrière, N., Riad, M., Dal Bo, G., Lévesque, D., Trudeau, L.E., and Descarries, L. (2009). The dual dopamine-glutamate phenotype of growing mesencephalic neurons regresses in mature rat brain. J. Comp. Neurol. *517*, 873–891.

Birgner, C., Nordenankar, K., Lundblad, M., Mendez, J.A., Smith, C., le Grevès, M., Galter, D., Olson, L., Fredriksson, A., Trudeau, L.E., et al. (2010). VGLUT2 in dopamine neurons is required for psychostimulant-induced behavioral activation. Proc. Natl. Acad. Sci. USA *107*, 389–394.

Blumstein, J., Faundez, V., Nakatsu, F., Saito, T., Ohno, H., and Kelly, R.B. (2001). The neuronal form of adaptor protein-3 is required for synaptic vesicle formation from endosomes. J. Neurosci. *21*, 8034–8042.

Bolte, S., and Cordelières, F.P. (2006). A guided tour into subcellular colocalization analysis in light microscopy. J. Microsc. *224*, 213–232.

Brimblecombe, K.R., Gracie, C.J., Platt, N.J., and Cragg, S.J. (2015). Gating of dopamine transmission by calcium and axonal N-, Q-, T- and L-type voltage-gated calcium channels differs between striatal domains. J. Physiol. *593*, 929–946.

Chaudhry, F.A., Reimer, R.J., Bellocchio, E.E., Danbolt, N.C., Osen, K.K., Edwards, R.H., and Storm-Mathisen, J. (1998). The vesicular GABA transporter, VGAT, localizes to synaptic vesicles in sets of glycinergic as well as GABAergic neurons. J. Neurosci. *18*, 9733–9750.

Chi, P., Greengard, P., and Ryan, T.A. (2001). Synapsin dispersion and reclustering during synaptic activity. Nat. Neurosci. *4*, 1187–1193.

Dittman, J.S., Kreitzer, A.C., and Regehr, W.G. (2000). Interplay between facilitation, depression, and residual calcium at three presynaptic terminals. J. Neurosci. *20*, 1374–1385.

Eggermann, E., Bucurenciu, I., Goswami, S.P., and Jonas, P. (2011). Nanodomain coupling between Ca^{2+} channels and sensors of exocytosis at fast mammalian synapses. Nat. Rev. Neurosci. *13*, 7–21.

El Mestikawy, S., Wallén-Mackenzie, A., Fortin, G.M., Descarries, L., and Trudeau, L.E. (2011). From glutamate co-release to vesicular synergy: vesicular glutamate transporters. Nat. Rev. Neurosci. *12*, 204–216.

Eriksen, J., Rasmussen, S.G., Rasmussen, T.N., Vaegter, C.B., Cha, J.H., Zou, M.F., Newman, A.H., and Gether, U. (2009). Visualization of dopamine transporter trafficking in live neurons by use of fluorescent cocaine analogs. J. Neurosci. *29*, 6794–6808.

Evstratova, A., Chamberland, S., Faundez, V., and Tóth, K. (2014). Vesicles derived via AP-3-dependent recycling contribute to asynchronous release and influence information transfer. Nat. Commun. *5*, 5530.

Faúndez, V., Horng, J.T., and Kelly, R.B. (1997). ADP ribosylation factor 1 is required for synaptic vesicle budding in PC12 cells. J. Cell Biol. *138*, 505–515.

Faúndez, V., Horng, J.T., and Kelly, R.B. (1998). A function for the AP3 coat complex in synaptic vesicle formation from endosomes. Cell *93*, 423–432.

Fon, E.A., Pothos, E.N., Sun, B.-C., Killeen, N., Sulzer, D., and Edwards, R.H. (1997). Vesicular transport regulates monoamine storage and release but is not essential for amphetamine action. Neuron *19*, 1271–1283.

Fortin, G.M., Ducrot, C., Giguère, N., Kouwenhoven, W.M., Bourque, M.J., Pacelli, C., Varaschin, R.K., Brill, M., Singh, S., Wiseman, P.W., and Trudeau, L.É. (2019). Segregation of dopamine and glutamate release sites in dopamine neuron axons: regulation by striatal target cells. FASEB J. *33*, 400–417.

Foss, S.M., Li, H., Santos, M.S., Edwards, R.H., and Voglmaier, S.M. (2013). Multiple dileucine-like motifs direct VGLUT1 trafficking. J. Neurosci. *33*, 10647–10660.

Fredj, N.B., and Burrone, J. (2009). A resting pool of vesicles is responsible for spontaneous vesicle fusion at the synapse. Nat. Neurosci. *12*, 751–758.

Goh, G.Y., Huang, H., Ullman, J., Borre, L., Hnasko, T.S., Trussell, L.O., and Edwards, R.H. (2011). Presynaptic regulation of quantal size: K+/H+ exchange stimulates vesicular glutamate transport. Nat. Neurosci. *14*, 1285–1292.

Gong, S., Yang, X.W., Li, C., and Heintz, N. (2002). Highly efficient modification of bacterial artificial chromosomes (BACs) using novel shuttle vectors containing the R6Kgamma origin of replication. Genome Res. *12*, 1992–1998.

Gras, C., Amilhon, B., Lepicard, E.M., Poirel, O., Vinatier, J., Herbin, M., Dumas, S., Tzavara, E.T., Wade, M.R., Nomikos, G.G., et al. (2008). The vesicular glutamate transporter VGLUT3 synergizes striatal acetylcholine tone. Nat. Neurosci. *11*, 292–300.

Groemer, T.W., and Klingauf, J. (2007). Synaptic vesicles recycling spontaneously and during activity belong to the same vesicle pool. Nat. Neurosci. *10*, 145–147.

Härtig, W., Riedel, A., Grosche, J., Edwards, R.H., Fremeau, R.T., Jr., Harkany, T., Brauer, K., and Arendt, T. (2003). Complementary distribution of vesicular glutamate transporters 1 and 2 in the nucleus accumbens of rat: Relationship to calretinin-containing extrinsic innervation and calbindin-immunoreactive neurons. J. Comp. Neurol. *465*, 1–10.

Hattori, T., Takada, M., Moriizumi, T., and Van der Kooy, D. (1991). Single dopaminergic nigrostriatal neurons form two chemically distinct synaptic types: possible transmitter segregation within neurons. J. Comp. Neurol. *309*, 391–401.

Hnasko, T.S., and Edwards, R.H. (2012). Neurotransmitter corelease: mechanism and physiological role. Annu. Rev. Physiol. *74*, 225–243.

Hnasko, T.S., Chuhma, N., Zhang, H., Goh, G.Y., Sulzer, D., Palmiter, R.D., Rayport, S., and Edwards, R.H. (2010). Vesicular glutamate transport promotes dopamine storage and glutamate corelease in vivo. Neuron *65*, 643–656.

Howe, M.W., and Dombeck, D.A. (2016). Rapid signalling in distinct dopaminergic axons during locomotion and reward. Nature *535*, 505–510.

Hua, Y., Sinha, R., Martineau, M., Kahms, M., and Klingauf, J. (2010). A common origin of synaptic vesicles undergoing evoked and spontaneous fusion. Nat. Neurosci. *13*, 1451–1453.

Hua, Z., Leal-Ortiz, S., Foss, S.M., Waites, C.L., Garner, C.C., Voglmaier, S.M., and Edwards, R.H. (2011). v-SNARE composition distinguishes synaptic vesicle pools. Neuron *71*, 474–487.

Jonas, P., Bischofberger, J., and Sandkühler, J. (1998). Corelease of two fast neurotransmitters at a central synapse. Science *281*, 419–424.

Kantheti, P., Qiao, X., Diaz, M.E., Peden, A.A., Meyer, G.E., Carskadon, S.L., Kapfhamer, D., Sufalko, D., Robinson, M.S., Noebels, J.L., and Burmeister, M. (1998). Mutation in AP-3 delta in the mocha mouse links endosomal transport to storage deficiency in platelets, melanosomes, and synaptic vesicles. Neuron *21*, 111–122.

Kawano, M., Kawasaki, A., Sakata-Haga, H., Fukui, Y., Kawano, H., Nogami, H., and Hisano, S. (2006). Particular subpopulations of midbrain and hypothalamic dopamine neurons express vesicular glutamate transporter 2 in the rat brain. J. Comp. Neurol. *498*, 581–592.

Kennedy, R.T., Jones, S.R., and Wightman, R.M. (1992). Dynamic observation of dopamine autoreceptor effects in rat striatal slices. J. Neurochem. *59*, 449–455.

Kim, S.H., and Ryan, T.A. (2009). A distributed set of interactions controls μ2 functionality in AP-2's role as a sorting adaptor in synaptic vesicle endocytosis. J. Biol. Chem. *284*, 32803–32812.

Kim, S.H., and Ryan, T.A. (2010). CDK5 serves as a major control point in neurotransmitter release. Neuron *67*, 797–809.

Kononenko, N.L., Puchkov, D., Classen, G.A., Walter, A.M., Pechstein, A., Sawade, L., Kaempf, N., Trimbuch, T., Lorenz, D., Rosenmund, C., et al. (2014). Clathrin/AP-2 mediate synaptic vesicle reformation from endosome-like vacuoles but are not essential for membrane retrieval at central synapses. Neuron *82*, 981–988.

Koranda, J.L., Cone, J.J., McGehee, D.S., Roitman, M.F., Beeler, J.A., and Zhuang, X. (2014). Nicotinic receptors regulate the dynamic range of dopamine release in vivo. J. Neurophysiol. *111*, 103–111.

Lamotte d'Incamps, B., Bhumbra, G.S., Foster, J.D., Beato, M., and Ascher, P. (2017). Segregation of glutamatergic and cholinergic transmission at the mixed motoneuron Renshaw cell synapse. Sci. Rep. *7*, 4037.

Lee, S., Kim, K., and Zhou, Z.J. (2010). Role of ACh-GABA cotransmission in detecting image motion and motion direction. Neuron *68*, 1159–1172.

Li, P., Merrill, S.A., Jorgensen, E.M., and Shen, K. (2016). Two clathrin adaptor protein complexes instruct axon-dendrite polarity. Neuron *90*, 564–580.

Li, H., Santos, M.S., Park, C.K., Dobry, Y., and Voglmaier, S.M. (2017). VGLUT2 Trafficking Is Differentially Regulated by Adaptor Proteins AP-1 and AP-3. Front. Cell. Neurosci. *11*, 324.

Liu, C., Kershberg, L., Wang, J., Schneeberger, S., and Kaeser, P.S. (2018). Dopamine secretion Is mediated by sparse active zone-like release sites. Cell *172*, 706–718.

Logan, T., Bendor, J., Toupin, C., Thorn, K., and Edwards, R.H. (2017). α-Synuclein promotes dilation of the exocytotic fusion pore. Nat. Neurosci. *20*, 681–689.

Marcott, P.F., Mamaligas, A.A., and Ford, C.P. (2014). Phasic dopamine release drives rapid activation of striatal D2-receptors. Neuron *84*, 164–176.

Martinez-Arca, S., Alberts, P., Zahraoui, A., Louvard, D., and Galli, T. (2000). Role of tetanus neurotoxin insensitive vesicle-associated membrane protein (TI-VAMP) in vesicular transport mediating neurite outgrowth. J. Cell Biol. *149*, 889–900.

Midorikawa, M., Tsukamoto, Y., Berglund, K., Ishii, M., and Tachibana, M. (2007). Different roles of ribbon-associated and ribbon-free active zones in retinal bipolar cells. Nat. Neurosci. *10*, 1268–1276.

Miesenböck, G., De Angelis, D.A., and Rothman, J.E. (1998). Visualizing secretion and synaptic transmission with pH-sensitive green fluorescent proteins. Nature *394*, 192–195.

Nelson, A.B., Bussert, T.G., Kreitzer, A.C., and Seal, R.P. (2014). Striatal cholinergic neurotransmission requires VGLUT3. J. Neurosci. *34*, 8772–8777.

Newell-Litwa, K., Chintala, S., Jenkins, S., Pare, J.F., McGaha, L., Smith, Y., and Faundez, V. (2010). Hermansky-Pudlak protein complexes, AP-3 and BLOC-1, differentially regulate presynaptic composition in the striatum and hippocampus. J. Neurosci. *30*, 820–831.

Nirenberg, M.J., Chan, J., Liu, Y., Edwards, R.H., and Pickel, V.M. (1997). Vesicular monoamine transporter-2: immunogold localization in striatal axons and terminals. Synapse *26*, 194–198.

Nirenberg, M.J., Chan, J., Liu, Y., Edwards, R.H., and Pickel, V.M. (1998). Ultrastructural localization of the vesicular monoamine transporter 2 in mesolimbic and nigrostriatal dopaminergic neurons. Adv. Pharmacol. *42*, 240–243.

Onoa, B., Li, H., Gagnon-Bartsch, J.A., Elias, L.A., and Edwards, R.H. (2010). Vesicular monoamine and glutamate transporters select distinct synaptic vesicle recycling pathways. J. Neurosci. *30*, 7917–7927.

Pan, P.Y., and Ryan, T.A. (2012). Calbindin controls release probability in ventral tegmental area dopamine neurons. Nat. Neurosci. *15*, 813–815.

Pan, P.Y., Marrs, J., and Ryan, T.A. (2015). Vesicular glutamate transporter 1 orchestrates recruitment of other synaptic vesicle cargo proteins during synaptic vesicle recycling. J. Biol. Chem. *290*, 22593–22601.

Peters, A., Palay, S.L., and Webster, H.d. (1970). The Fine Structure of the Nervous System Neurons and their Supporting Cells. (Oxford University Press).

Phillips, P.E., and Stamford, J.A. (2000). Differential recruitment of N-, P- and Q-type voltage-operated calcium channels in striatal dopamine release evoked by 'regular' and 'burst' firing. Brain Res. *884*, 139–146.

Phillips, P.E., Hancock, P.J., and Stamford, J.A. (2002). Time window of autoreceptor-mediated inhibition of limbic and striatal dopamine release. Synapse *44*, 15–22.

Ramirez, D.M., and Kavalali, E.T. (2011). Differential regulation of spontaneous and evoked neurotransmitter release at central synapses. Curr. Opin. Neurobiol. *21*, 275–282.

Ramirez, D.M., Khvotchev, M., Trauterman, B., and Kavalali, E.T. (2012). Vti1a identifies a vesicle pool that preferentially recycles at rest and maintains spontaneous neurotransmission. Neuron *73*, 121–134.

Ren, J., Qin, C., Hu, F., Tan, J., Qiu, L., Zhao, S., Feng, G., and Luo, M. (2011). Habenula "cholinergic" neurons co-release glutamate and acetylcholine and activate postsynaptic neurons via distinct transmission modes. Neuron *69*, 445–452.

Rizzoli, S.O., and Betz, W.J. (2005). Synaptic vesicle pools. Nat. Rev. Neurosci. *6*, 57–69.

Saheki, Y., and De Camilli, P. (2012). Synaptic vesicle endocytosis. Cold Spring Harb. Perspect. Biol. *4*, a005645.

Salazar, G., Love, R., Werner, E., Doucette, M.M., Cheng, S., Levey, A., and Faundez, V. (2004). The zinc transporter ZnT3 interacts with AP-3 and it is preferentially targeted to a distinct synaptic vesicle subpopulation. Mol. Biol. Cell *15*, 575–587.

Salazar, G., Craige, B., Love, R., Kalman, D., and Faundez, V. (2005). Vglut1 and ZnT3 co-targeting mechanisms regulate vesicular zinc stores in PC12 cells. J. Cell Sci. *118*, 1911–1921.

Sara, Y., Virmani, T., Deák, F., Liu, X., and Kavalali, E.T. (2005). An isolated pool of vesicles recycles at rest and drives spontaneous neurotransmission. Neuron *45*, 563–573.

Schermelleh, L., Carlton, P.M., Haase, S., Shao, L., Winoto, L., Kner, P., Burke, B., Cardoso, M.C., Agard, D.A., Gustafsson, M.G., et al. (2008). Subdiffraction multicolor imaging of the nuclear periphery with 3D structured illumination microscopy. Science *320*, 1332–1336.

Scheuber, A., Rudge, R., Danglot, L., Raposo, G., Binz, T., Poncer, J.C., and Galli, T. (2006). Loss of AP-3 function affects spontaneous and evoked release at hippocampal mossy fiber synapses. Proc. Natl. Acad. Sci. USA *103*, 16562–16567.

Schultz, W., Dayan, P., and Montague, P.R. (1997). A neural substrate of prediction and reward. Science *275*, 1593–1599.

Sengupta, A., Bocchio, M., Bannerman, D.M., Sharp, T., and Capogna, M. (2017). Control of amygdala circuits by 5-HT neurons via 5-HT and glutamate cotransmission. J. Neurosci. *37*, 1785–1796.

Shin, J.H., Adrover, M.F., and Alvarez, V.A. (2017). Distinctive modulation of dopamine release in the nucleus accumbens shell mediated by dopamine and acetylcholine receptors. J. Neurosci. *37*, 11166–11180.

Sirkis, D.W., Edwards, R.H., and Asensio, C.S. (2013). Widespread dysregulation of peptide hormone release in mice lacking adaptor protein AP-3. PLoS Genet. *9*, e1003812.

Strasser, J.E., Arribas, M., Blagoveshchenskaya, A.D., and Cutler, D.F. (1999). Secretagogue-triggered transfer of membrane proteins from neuroendocrine secretory granules to synaptic-like microvesicles. Mol. Biol. Cell *10*, 2619–2630.

Sulzer, D., Joyce, M.P., Lin, L., Geldwert, D., Haber, S.N., Hattori, T., and Rayport, S. (1998). Dopamine neurons make glutamatergic synapses in vitro. J. Neurosci. *18*, 4588–4602.

Sulzer, D., Cragg, S.J., and Rice, M.E. (2016). Striatal dopamine neurotransmission: regulation of release and uptake. Basal Ganglia *6*, 123–148.

Takács, V.T., Cserép, C., Schlingloff, D., Pósfai, B., Szőnyi, A., Sos, K.E., Környei, Z., Dénes, Á., Gulyás, A.I., Freund, T.F., and Nyiri, G. (2018). Co-transmission of acetylcholine and GABA regulates hippocampal states. Nat. Commun. *9*, 2848.

Takahashi, N., Miner, L.L., Sora, I., Ujike, H., Revay, R.S., Kostic, V., Jackson-Lewis, V., Przedborski, S., and Uhl, G.R. (1997). VMAT2 knockout mice: heterozygotes display reduced amphetamine-conditioned reward, enhanced amphetamine locomotion, and enhanced MPTP toxicity. Proc. Natl. Acad. Sci. USA *94*, 9938–9943.

Tan, P.K., Waites, C., Liu, Y., Krantz, D.E., and Edwards, R.H. (1998). A leucine-based motif mediates the endocytosis of vesicular monoamine and acetylcholine transporters. J. Biol. Chem. *273*, 17351–17360.

Tritsch, N.X., Ding, J.B., and Sabatini, B.L. (2012). Dopaminergic neurons inhibit striatal output through non-canonical release of GABA. Nature *490*, 262–266.

Tritsch, N.X., Granger, A.J., and Sabatini, B.L. (2016). Mechanisms and functions of GABA co-release. Nat. Rev. Neurosci. *17*, 139–145.

van de Bospoort, R., Farina, M., Schmitz, S.K., de Jong, A., de Wit, H., Verhage, M., and Toonen, R.F. (2012). Munc13 controls the location and efficiency of dense-core vesicle release in neurons. J. Cell Biol. *199*, 883–891.

Voglmaier, S.M., Kam, K., Yang, H., Fortin, D.L., Hua, Z., Nicoll, R.A., and Edwards, R.H. (2006). Distinct endocytic pathways control the rate and extent of synaptic vesicle protein recycling. Neuron *51*, 71–84.

Wang, Y.-M., Gainetdinov, R.R., Fumagalli, F., Xu, F., Jones, S.R., Bock, C.B., Miller, G.W., Wightman, R.M., and Caron, M.G. (1997). Knockout of the vesicular monoamine transporter 2 gene results in neonatal death and supersensitivity to cocaine and amphetamine. Neuron *19*, 1285–1296.

Watanabe, S., Trimbuch, T., Camacho-Pérez, M., Rost, B.R., Brokowski, B., Söhl-Kielczynski, B., Felies, A., Davis, M.W., Rosenmund, C., and Jorgensen, E.M. (2014). Clathrin regenerates synaptic vesicles from endosomes. Nature *515*, 228–233.

Zhang, S., Qi, J., Li, X., Wang, H.L., Britt, J.P., Hoffman, A.F., Bonci, A., Lupica, C.R., and Morales, M. (2015). Dopaminergic and glutamatergic microdomains in a subset of rodent mesoaccumbens axons. Nat. Neurosci. *18*, 386–392.

STAR★METHODS

KEY RESOURCES TABLE

REAGENT or RESOURCE	SOURCE	IDENTIFIER
Antibodies		
guinea pig anti-VGLUT2	Millipore	AB2251; RRID:AB_2665454
mouse anti-HA11	Covance	MMS-101R; RRID:AB_291262
rat anti-HA	Roche	11867423001; RRID:AB_10094468
chicken anti-GFP	Invitrogen	10262; RRID:AB_2534023
mouse anti-TH	Millipore	MAB5280; RRID:AB_2201526
rabbit anti-TH	Millipore	AB152; RRID:AB_390204
mouse anti-AP3 delta	Hybridoma Bank	AB2056641; RRID:AB_2056641
chicken anti-piccolo	Synaptic Systems	142 116; RRID:AB_2661778
chicken anti-bassoon	Synaptic Systems	141 016; RRID:AB_2661779
rabbit anti-munc13-1	Synaptic Systems	126 103; RRID:AB_887733
mouse anti-SV2	Hybridoma Bank	AB2315387; RRID:AB_2315387
Alexa 488 anti-chicken	Invitrogen	11039
Alexa 488 anti-guinea pig	Invitrogen	11073
Alexa 488 anti-mouse	Invitrogen	11029
Alexa 488 anti-rabbit	Invitrogen	11008
Alexa 488 anti-rat	Invitrogen	21208
Alexa 546 anti-chicken	Invitrogen	11040
Alexa 546 anti-guinea pig	Invitrogen	11074
Alexa 546 anti-mouse	Invitrogen	11030
Alexa 546 anti-rabbit	Invitrogen	11035
Alexa 546 anti-rat	Invitrogen	11081
Alexa 635 anti-mouse	Invitrogen	31575
Alexa 647 anti-rabbit	Invitrogen	21244
Alexa 647 anti-rat	Invitrogen	21247
Bacterial and Virus Strains		
AAV5-Ef1alfa-DIO-VGLUT2-HA-WPRE	UNC Vector Core	N/A
AAV9-hSynapsin-DIO-VGLUT2-pHluorin-WPRE	Penn Vector Core	N/A
AAV2/9-hSynapsin-tdTomato-T2A-mGIRK2-1-A22A-WPRE	Penn Vector Core	N/A
AAV5-EF1α-DIO-ChR2-mCherry	UNC Vector Core	N/A
Chemicals, Peptides, and Recombinant Proteins		
w-Agatoxin TK	Alomone	STA-530
w-conotoxin GVIA	Alomone	C-300
Bafilomycin A1	Calbiochem	196000
Picrotoxin	Sigma	P1675
EGTA/AM	EMD Millipore	324628
CGP55845	Sigma	SML0594
scopolamine hydrobromide	Sigma	PHR1470
SCH 23390	Sigma	D054
CNQX disodium salt	Abcam	ab120044
DL-AP5 sodium salt	Abcam	ab120271
Tetrabenazine	Tocris	2175
(+)-a-dihydrotetrabenazine [9-O-methyl-3H]	ARC	ART 2119

(*Continued on next page*)

Continued		
REAGENT or RESOURCE	SOURCE	IDENTIFIER
a-methyl-*p*-tyrosine methyl ester hydrochloride (AMPT)	Sigma	120693
JHC 1-64	Amy Newman lab	PMID: 19474307
Experimental Models: Organisms/Strains		
B6;129S6-*Gt(ROSA)26Sor*$^{tm9(CAG-tdTomato)Hze}$/J mouse	The Jackson Laboratory	JAX: 007905; RRID:IMSR_JAX:007905
DAT ires-Cre mouse	The Jackson Laboratory	JAX: 006660; RRID:IMSR_JAX:006660
C57BL/6 mouse	The Jackson Laboratory	JAX: 000664; RRID:IMSR_JAX:000664
HA-VMAT2 Bac transgenic mouse	This paper	N/A
Oligonucleotides		
HA-VMAT2 genotyping forward primer: CTACGACGT CCCCGACTACG	This paper	N/A
HA-VMAT2 genotyping reverse primer: CAAGAGTGC CCAGTTTATGTAG	This paper	N/A
Recombinant DNA		
pFUGW-VGLUT2-pHluorin	Foss et al., 2013	N/A
pFUGW-VMAT2-pHluorin	Logan et al., 2017	N/A
pFUGW-VMAT2-mOrange2	This paper	N/A
Software and Algorithms		
Prism 6	GraphPad	https://www.graphpad.com/scientific-software/prism/
ImageJ	https://imagej.net/contributors	https://imagej.nih.gov/ij/download.html
Metamorph	Molecular Devices	https://www.moleculardevices.com/products/cellular-imaging-systems/acquisition-and-analysis-software/metamorph-microscopy#gref
Clampfit 10.3	Molecular Devices	http://mdc.custhelp.com/app/answers/detail/a_id/18779/~/axon™pclamp™-10-electrophysiology-data-acquisition-%26-analysis-software-download
Nikon Elements	Nikon	https://www.microscope.healthcare.nikon.com/products/software/nis-elements
Micro-Manager	micro-manager.org	https://micro-manager.org/wiki/Download_Micro-Manager_Latest_Release
Illustrator	Adobe	https://www.adobe.com/products/illustrator.html?promoid=PGRQQLFS&mv=other

CONTACT FOR REAGENT AND RESOURCE SHARING

Further information and requests for resources and reagents should be directed to and will be fulfilled by the Lead Contact, Robert H. Edward (Robert.Edward@ucsf.edu).

EXPERIMENTAL MODEL AND SUBJECT DETAILS

Mice

Both male and female mice were used for all experiments. All mice received unlimited food and water and were exposed to 12h/12h light/dark cycle. DAT iCre/+ heterozygous mice were used for stereotactic injections of conditional AAVs at 3-4 weeks of age in animals used for electrophysiology and at 2 months of age in animals used for anatomy. Mice were allowed to recover for at least 3 weeks before further procedures. All experiments with animals were performed according to the National Institutes of Health Guide for Care and Use of Laboratory Animals and were approved by the University of California San Francisco Institutional Animal Care and Use Committee.

Generation of HA-VMAT2 BAC transgenic mice

Bacterial artificial chromosome (BAC) BAC23-233F7 containing the entire mouse genome was modified using a two-step procedure (Gong et al., 2002). Overlap extension PCR was used to insert the hemagglutinin (HA) epitope tag into the large lumenal loop between transmembrane domains 1 and 2 at a site previously described (Tan et al., 1998), as well as to amplify surrounding regions, and this

PCR product was cloned into shuttle vector pLD53 conferring ampicillin resistance and sucrose sensitivity. The resulting shuttle vector was electroporated into host bacteria containing the BAC (conferring chloramphenicol resistance), selected with ampicillin and chloramphenicol and potential cointegrates screened by PCR. Positive clones were submitted to double selection with chloramphenicol and sucrose and potentially resolved BAC clones identified by PCR and confirmed by Southern analysis. The integrity of the modified BAC was assessed by restriction digest and compared to the original unmodified BAC. Modified BAC DNAs were then diluted into polyamine microinjection buffer and microinjected into C57/Bl6J eggs at the Gladstone Institutes Transgenic Core Facility (San Francisco). Transgenic offspring were identified by PCR for the HA tag, three founders identified and mated to C57BL/6J mice. Two of the founders transmitting the transgene with the expected mendelian ratio expressed HA-VMAT2 at low or undetectable levels. The third founder transmitted with low frequency (1/29 offspring), suggesting chimerism, but subsequent transmission occurred at mendelian ratios with robust expression of HA-VMAT2.

Primary culture

Hippocampal neurons

Hippocampi were dissected from P0 mice of both sexes, dissociated in 0.25% trypsin, washed three times with Hank's Balanced Salt Solution (HBSS) containing 10 mM HEPES and 20 mM glucose, triturated and plated on poly-L-lysine coated coverslips at 350 cells/mm^2. Neurons were plated in Minimal Essential Medium containing 1x B27 (GIBCO, 17504-044), 2 mM glutamax (GIBCO, 35050-061), 5% FBS (HyClone, defined), 21 mM glucose (Sigma, G8769) and 1x penicillin/streptomycin (Corning, 30-002-CL). After one day *in vitro* (DIV1), 3/4 of the medium was changed to Neurobasal (GIBCO, 21103-049) with B27, glutamax and penicillin/streptomycin. Cells were infected with lentiviruses encoding VGLUT2-pHluorin, VMAT2-pHluorin or VGLUT2-pHluorin + VMAT2-mOrange2 on DIV 4. Cytosine arabinoside at 4 μM was added on DIV7 to inhibit glial proliferation.

Dopamine neurons

Ventral midbrain region containing substantia nigra and ventral tegmental area was dissected from neonatal DAT iCre/B6;129S6-Gt(ROSA)26Sor$^{tm9(CAG-tdTomato)Hze}$/J, wild-type or *mocha* mice of both sexes. *Mocha* mice were compared to littermate controls. Tissue pieces were dissociated in papain for 15 minutes, washed with HBSS containing 10 mM HEPES and 20 mM glucose, triturated and plated on astrocyte monolayers at 1000 cells/mm^2 in medium containing 60% Neurobasal-A, 30% Basal Media Eagle, 10% fetal bovine serum (HyClone, defined), 1x B27, 2 mM GlutaMAX, 10 ng/mL glial cell line-derived neurotrophic factor (Millipore, MA, USA) and 1x penicillin/streptomycin. Cells were infected with lentiviruses encoding VGLUT2-pHluorin or VMAT2-pHluorin on DIV 2.

METHOD DETAILS

Stereotactic virus injection

Anesthesia was induced and maintained with inhaled isoflurane (2%). For the slice recording, DAT-Cre/+ mice (Slc6a3cre) were injected at 200 nL/min with 400 nL recombinant adeno-associated virus (AAV) encoding double floxed channelrhodopsin-2 (ChR2) (AAV5-EF1α-DIO-ChR2-mCherry) into the ventral tegmental area (coordinates in mm relative to bregma, −3.25 anteroposterior, −4.40 dorsoventral, and ± 0.5 mediolateral) and with 300 nL AAV encoding GIRK2 (AAV2/9.hSynapsin.tdTomato.T2A.mGIRK2-1-A22A.WPRE diluted 1:3 in PBS) into the medial shell of the nucleus accumbens (+1.00 anteroposterior, −4.40 dorsoventral, and ± 0.75 mediolateral). For the anatomy, DAT-Cre/+ or DAT-Cre/+/HA-VMAT2 mice were injected with 500 nL AAV5-EF1α-DIO-HA-VGLUT2 or AAV9-syn-DIO-VGLUT2-pHluorin respectively in the VTA.

Immunohistochemistry

Mice were perfused with 4% PFA in PBS, the brains postfixed overnight in 4% PFA and cryoprotected in PBS containing 30% sucrose. Sections (35 μm) were cut using a Leica CM3050 S cryostat. Cultured cells were fixed for 10 minutes in 4% PFA in PBS and washed three times in PBS. Floating sections as well as cultured cells were blocked and permeabilized in PBS containing 4% normal goat serum and 0,2% Triton X-100. Primary and secondary antibodies were diluted in PBS containing 1% normal goat serum and 0.2% Triton X-100 in PBS for staining slices and in 1% normal goat serum in PBS for staining cultured cells. Primary antibodies were incubated overnight at 4°C and secondary antibodies at room temperature for 2 hours in the dark. Slices were mounted in Fluoromount-G (SouthernBiotech) or Vectashield (Vector Laboratories). Antibodies were used at the following dilutions: guinea pig anti-VGLUT2 1/2000, mouse and rabbit anti-TH 1/1000, all other primary antibodies at 1/500. All secondary antibodies were used at 1/500 dilution.

Images were acquired using the Nikon Ti Microscope equipped with CSU-W1 spinning disk confocal, Andor Zyla sCMOS camera and a Plan Apo VC 100x/1.4 oil objective or with N-SIM module, Andor DU-897 EMCCD camera and Apo TIRF 100x/1.49 Oil objective. Lasers (488 nm, 561 nm and 640 nm) were used for excitation and ET525/50, ET600/50 and ET700/75 filters for emission. For midbrain cultures, tyrosine hydroxylase staining was used as mask and colocalization with different markers was calculated only in TH$^+$ cells. JACoP plugin (Bolte and Cordelières, 2006) in ImageJ was used to determine colocalization coefficients.

Slice electrophysiology

Slice preparation

Three to eight weeks after virus injection, mice were deeply anesthetized with intraperitoneal ketamine/xylazine and transcardially perfused with cold artificial cerebrospinal fluid (ACSF) containing (in mM) 119 NaCl, 2.5 KCl, 1.3 $MgSO_4$, 2.5 $CaCl_2$, 26 $NaHCO_3$, 1 NaH_2PO_4, and 11 D-glucose (315 Osm, pH 7.4), then decapitated. The brains were removed and cut on a vibratome (Leica) in aerated (95% O_2, 5% CO_2), cold slicing solution that contained (in mM): 110 choline chloride, 2.5 KCl, 7 $MgSO_4$, 0.5 $CaCl_2$, 1.25 NaH_2PO_4, 25 $NaHCO_3$, 25 D-glucose, 11.6 Na ascorbate and 3.1 Na pyruvate. Slices were incubated at 35°C for a minimum of 30 minutes in aerated ACSF. Nucleus accumbens slices were visualized with an upright infrared differential interference contrast (IR-DIC) microscope (BX50WI; Olympus) and perfused with aerated ACSF at room temperature throughout recording. Picrotoxin (100 μM), CGP55845 (300 nM), scopolamine hydrobromide (200 nM), and SCH 23390 hydrochloride (1 μM) (all obtained from Sigma) were added to the ACSF to isolate glutamate receptor- and D2 dopamine receptor-mediated currents. The D2 antagonist sulpiride (1 μM) was also added to isolate the glutamate-mediated EPSCs, but its omission did not reduce the extent of synaptic depression in response to trains (data not shown). ω-Agatoxin TK and ω-conotoxin GVIA (both from Alomone) were used to assess dependence on P-/Q-type and N-type Ca^{2+} channels.

Whole cell recordings

Whole cell voltage clamp recordings (V_h = −70 mV) were made from tdTomato$^+$ spiny projection neurons (SPNs) in the shell of the nucleus accumbens. Glass electrodes (3-5 MΩ) contained 115 mM K methanesulphonate, 20 mM NaCl, 1.5 mM $MgCl_2$, 10 mM HEPES-KOH, 10 mM tetrapotassium BAPTA, 1 mg/ml ATP, 0.1 mg/ml GTP, 1.5 mg/ml phosphocreatine and 5 mM QX314 (pH 7.4, 275 mOsm) to record glutamate receptor- and D2 receptor-mediated currents; or cesium methanesulfonate-based internal solution containing (in mM) 136 $CsMeSO_4$, 7 CsCl, 0.25 EGTA, 10 HEPES, 2 MgATP, 0.3 Na_2GTP, 8 NaCl, 0.1 spermine, 7 phosphocreatine and 5 QX314 to isolate glutamate receptor-mediated currents. Field blue light (488 nm, pulse width 2-5 ms) was applied through a 40x objective to excite ChR2. The D2-IPSC was measured by subtracting the baseline (1- 20 ms before the first stimulus) from the peak amplitude of the IPSC. Sensitivity to TBZ (Tocris) was determined before and after 30 min bath incubation.

Measurement of monoamine levels

Age- and weight-matched adult male and female mice (~25 g) were divided into two groups and injected intraperitoneally with α-methyl-*p*-tyrosine methyl ester hydrochloride (AMPT,100 mg/kg) or saline 24, 20, and 4 h before either slice recording or the measurement of monoamine content. To measure tissue monoamine after treatment with AMPT, the nucleus accumbens was isolated from slices prepared as above, frozen on dry ice and stored at −80°C. To measure monoamine levels in wild-type and *mocha* mice, age-matched animals were euthanized by CO_2 inhalation, decapitated, the ventral and dorsal striata dissected in HBSS and immediately frozen on dry ice. Tissue catecholamine levels were measured by HPLC with coupled electrochemical detection at the Vanderbilt Neurochemistry Core.

[^{3}H]-Dihydrotetrabenazine binding

To dissect striatal tissue, the brains were placed into a rodent brain matrix (RBM-2000C, Protech International Inc.) and two 1 mm coronal slices collected. Cortical tissue was removed and striatal tissue collected in ice cold SHT buffer (320 mM sucrose, 10 mM HEPES/Tris pH 7.4) with 0.5 mM EDTA and Complete Protease Inhibitor Cocktail (Roche). Tissue from each striatum was disrupted with 12 strokes of a Dounce homogenizer at 500 rpm in ice cold SHT buffer. The sample was then sonicated for 30 s before sedimentation at 2000x g for 2 min. The pellet was discarded and the protein content of the supernatant determined by BCA. For the dihydrotetrabenazine binding, 50 μg membrane protein was incubated in SHT buffer with 10 nM (+)-a-dihydrotetrabenazine [9-O-methyl-^{3}H] (ARC; 80 Ci/mmol) for 30 minutes at 30°C. The reaction was stopped by filtration through a Supor 200 0.2 μm filter (PALL) and washed 3 times in ice-cold SHT buffer with 20 mM tetrabenazine (Fluka). Binding was done in triplicate for each sample and nonspecific binding determined in the presence of 10 μM non-radioactive tetrabenazine in the binding assay. Specific binding was normalized to the amount of membrane protein added to the reaction.

Live imaging

Hippocampal cultures between 16-19 DIV and dopamine neuron cultures between 14-16 DIV were mounted in a laminar flow perfusion and stimulation chamber on an inverted Nikon TE300 fluorescence microscope. Fluorescence signals were collected under epifluorescence illumination using the following bandpass filters: 470/40 nm excitation and 525/50 nm emission for pHluorin; 545/25 nm excitation and 605/70 nm emission for mOrange2, tdTomato or JHC 1-64. Midbrain cultures from wild-type and *mocha* mice were incubated for 10 min in fluorescent DAT ligand JHC 1-64 (30 nM) to visualize dopamine neurons (Eriksen et al., 2009). Cultures were then rinsed in imaging buffer before mounting in the chamber. All other midbrain cultures were made from DAT iCre/B6;129S6-Gt(ROSA)26Sor$^{tm9(CAG-tdTomato)Hze}$/J mice and dopamine neurons detected by the presence of cell-filling tdTomato. Dopamine neurons were located in the red channel and a single image acquired before switching to the pHluorin channel for imaging the response to stimulation. Images were acquired at 0.5 Hz in most experiments, and at 5 Hz for EGTA application. The frequency dependence and *mocha* experiments were imaged at 1 Hz. Action potentials (APs) were evoked by passing 1 ms bipolar current

pulses through platinum–iridium electrodes, to yield fields of 5–10 V/cm. Cells were continuously perfused with Tyrode's buffer (119 mM NaCl, 25 mM HEPES, 2 mM $CaCl_2$, 2 mM $MgCl_2$, 2.5 mM KCl, and 30 mM glucose at pH 7.4) containing 10 μM 6-cyano-7-nitroquinoxaline-2,3-dione (CNQX) and 10 μM 3-(2-carboxypiperazin-4-yl)propyl-1-phosphonic acid (APV). Imaging was done at room temperature in most experiments except for the analysis of frequency dependence in hippocampal and dopamine neurons, which was performed at 35°C. Total cellular pHluorin or mOrange2 content was revealed by applying Tyrode's buffer with 50 mM NH_4Cl, where NaCl was reduced to 69 mM. To measure exocytosis, Tyrode's solution with 600 nM Bafilomycin A1 (Calbiochem, 196000) was applied to cells just before starting the acquisition. To test the Ca^{2+} coupling of VMAT2- or VGLUT2-pHluorin exocytosis, cells were incubated for 3 minutes in 100 μM EGTA-AM (Calbiochem, 324628) or vehicle (0.1% DMSO).

QUANTIFICATION AND STATISTICAL ANALYSIS

Data analysis

Images were processed using ImageJ software. For most live imaging experiments, varicosities were manually selected based on fluorescence in buffer containing NH_4Cl. In dual color pHluorin/mOrange imaging varicosities in either channel were selected automatically using the granulometric filter in ImageJ. Background was subtracted and integrated fluorescence density in the varicosities was normalized to baseline before stimulation and to unquenched pHluorin fluorescence in NH_4Cl, or to maximal fluorescence after stimulation (as indicated in the text). Curves were fitted using GraphPad Prism 6 software.

Statistics

Statistical analysis of data was performed using GraphPad Prism 6 software. The D'Agostino & Pearson omnibus test was used to assess normality. The two-tailed unpaired t test was used for data with a normal distribution and the Mann-Whitney test for data that did not pass the test for normality. For multiple comparisons, ANOVA was used for the normally distributed data, and Kruskal-Wallis for the remainder.

DATA AND SOFTWARE AVAILABILITY

The datasets generated during and/or analyzed during the current study are available from the corresponding author on reasonable request.